Investigations into the Effect of Temperature on Power-line Corona using Bridge Measuring Techniques

Presented by:
Petrus Jacobus Pieterse

Prepared for:
Prof. C.T. Gaunt
Dept. of Electrical Engineering
University of Cape Town

Submitted to the Department of Electrical Engineering at the University of Cape Town in partial fulfilment of the academic requirements for a Master of Science in Engineering Specialising in Electrical Engineering

February 2023

Key words:
Power line corona, Conductor temperature, HTLS conductors, Bridge method

Declaration:

Iknow the meaning of plagiarism and declare that all the work in the document, save for that which is properly acknowledged, is my own. This dissertation has been submitted to the Turnitin module (or equivalent similarity and originality checking software) and I confirm that my supervisor has seen my report and any concerns revealed by such have been resolved with my supervisor.

Signed by candidate

Signed: P. J. Pieterse Date: 30.10.2023

Abstract

The need for more power and the limitations on building new power lines have made compact power lines a necessity. To design these lines, it is essential to understand the behavior of corona, which is a form of unwanted plasma discharge that causes electrical interference, power loss, and audible noise. Compact power lines require tighter conductor spacings and special high-temperature, low-sag conductors, which makes the accurate prediction of corona behavior even more crucial. This paper examines the impact of conductor temperature on corona performance, as it is an important factor that is often overlooked.

Despite earlier research showing that elevated conductor temperature has a direct effect on power line corona discharge magnitude, the effect of conductor temperature on corona performance is generally not considered since the line is not expected to remain at high temperatures for extended periods and since foul weather corona is considered worse. However, since high temperature low sag conductors may operate at much higher temperatures, the effect of temperature on the corona performance has to be considered. Earlier work has shown that simple correction factors based on the assumed local reduction of air density can be applied to predict the inception value for higher conductor temperatures. Likewise, the work of Chartier and Stearns showed a dependency of the corona noise measurement on the conductor temperature, albeit to only 50 °C. To date no relationship between conductor temperature and corona power losses has been published.

This dissertation demonstrates that losses for conductors exceeding 60 °C can be significant and follow a simple relationship with temperature. A new bridge detection method is introduced to evaluate corona loss performance by assessing positive and negative corona loss separately through post-processing of acquired data. The experiments were performed in a laboratory using a small coaxial conductor system or corona cage with a smooth aluminium heated center conductor ranging in temperature from 14 °C to 140 °C. The visible corona inception point is found to be lower than the point of rapid charge increase (as can be easily detected by the bridge circuit) which also follows approximately the Peek criteria with substitution of the ambient temperature for the conductor temperature, proving the bridge method to be more reliable than earlier visual observation methods.

This dissertation highlights the importance of considering the effect of conductor temperature on corona performance when designing compact power lines. By doing so, the detrimental impact of corona on practical systems can be minimized.

Contents

List of Figures

1 Introduction

High voltage power lines form a vital part of the Electrical Power System. Safe, reliable and efficient energy transmission and distribution requires that careful attention be paid, in particular, to the tower configuration and line design. The choice of tower and conductor configuration is normally based on standardised designs for a specific voltage and power capacity and is in general referred to as simply Line Design.

In present times greater demands are placed on Power Utilities as both the demand for power and the difficulty in obtaining right of way (servitude) is on the increase. When the construction of a new line is impossible, the only practical solution is to alter or retrofit an existing line by raising the system voltage or current or both. Since a specific tower design may not accommodate a higher system voltage or heavier conductors, a higher power density can only be achieved by increasing the conductor current density which will lead to higher than normal conductor temperatures. Steel-Reinforced Aluminium Conductors (ACSR), which are in common use, are typically rated for 93 °C and for short times as high as 150 °C with the maximum allowable sag being the main constraint. In an attempt to address the need for higher current densities, special high temperature low-sag alloy conductors have been developed to operate up to 280 °C.

Line sag or the height at midspan is not the only constraint for an acceptable design. Power line corona (unwanted plasma discharges on the line) needs to be controlled to maintain acceptable radio interference and audible noise levels and since very little design and operational experience is held to date for high temperature conductors, its corona performance is mostly unknown. The existing corona design model was developed when 75 °C was considered high for conductors, and therefore it may not prove adequate to predict the corona performance of high temperature conductors.

1.1 Motivation

Relatively little work has been done to date to study the effect of conductor temperature on corona performance. Most studies had shown that an increase in conductor temperature will increase the corona intensity and/or reduce the inception voltage thereof, however very little quantititive data is available.

In 1998, When I started my career in High voltage at the University of Stellenbosch, I was introduced to the well established field of Corona research led by Dr. J.P. Holtzhausen initially and after his retirement by Prof H. J. Vermeulen. This research group was later joined by members of the electromagnetic compatibility (EMC) research group under the guidance of Prof. H. C. Reader (which has led to the publishing of many interdisciplinary research). Discussions at conferences and within our groups had identified the lack of knowledge, specifically related to the effect of conductor temperature on corona performance which then led to the

initial studies on the topic.

Very early studies by F.W.Peek [2] on thin wires (2.6 - 4 mm) could not identify a correlation between conductor temperature and his Townsend based [3] corona prediction model. Results from graduate projects, using optical detection methods [4] however, identified that a correlation for corona inception is possible when substituting the air temperature for the conductor temperature similar to the method tried by Peek, but that a further experimentally obtained proportional correction factor is required. This work was published in 2010 at local and international conferences [5], [4] and later in 2014 [6] yielding different correction factors (possibly due to the subjective identification criteria used).

An attempt to (quantitatively) measure the accumulated charge [7] presented measurement difficulties (esp. w.r.t. negative corona) leading to inconclusive results. Filtering and inadequate sampling was identified as the main cause of the errors and consequently a capacitance bridge detection circuit, operating on the principle of charge integration, was developed [8] so as to measure the dissipated energy per cycle .

Similar work was performed by EPRI [9] in 2009 wherein a logarithmic correction function was proposed to calculate the gain in corona loss, radio interference voltage and audible noise as a function of the conductor temperature.

The discrepancy between the proportional correction factors obtained, using optical methods [4] [6] to find the inception voltage, coupled with the lack of technical details on the part of EPRI and the inconsistent results of Reid [7] then identified the need for further study in this field.

1.2 Research Method

The "Scientific Method" will be used.

A hypothesis was formed based on previous findings and observations, contemporary research will be reviewed and an experiment will be planned to support, or test the hypothesis respectively and to bridge the gaps identified.

1.2.1 Hypothesis

The main hypothesis is:
"A Higher conductor temperature creates an increase in ionising events which increases the number of free charges and consequently requires more work to be done by the external field in a unit of time; this translates to higher power loss."

1.2.2 Research Questions

This dissertation will aim to adress the following questions by means of a literature review and an experimental study:

- What are the physical characteristics of corona?
- What are the most important adverse effects of corona and do negative and positive corona have different impacts?
- which parameters are used to determine its severity
- What are the main factors which influence corona?
- What are the effects of higher conductor temperature on corona?
- How can corona be modeled and measured?

1.3 Chapter summary

This research dissertation is organised in Chapters, the contents of which can be summarised as follows.

Chapter 2 will address the main research questions, explain the underlying theories and provide a concise summary of past research.

Chapter 3 gives details regarding the test arrangement and the experimental design

Chapter 4 will summarise the main findings or research outcomes

Chapter 5 will discuss the results

2 Literature Review

2.1 Introduction

According to classical theory, gases have insulating properties when their molecules are in a neutral state, however, when charged particles are released to the gas from the electrodes or created within the gas (due to ionization), the gas will be in a higher state of matter, form a plasma and have an increased conductivity. In a uniform field, the onset of gas ionization usually leads to the establishment of a stable plasma channel or a complete breakdown, whereas in a non-uniform field, gas ionization can lead to locally confined gas discharges which can be transient or steady state in nature. These gas discharges are a type of partial discharge and are generally referred to as Corona.

The corona effect has been studied extensively, with one of the most noted reviews being that of Loeb [10]. The electrode configuration most commonly used is a sphere suspended above a flat plane or a hemisphere capped cylinder, referred to as the "standard" electrode [11], the tip radius and spacing of which can be scaled to achieve the required amount of non-uniformity while allowing for practical experimentation using some tens of kilovolts. A Journal publication using this type of electrode system and which is still frequently cited [12] shows the various types of coronas and has become a type of standard with regards to naming conventions.

Power lines suspended above ground; however, have a different field distribution and can have numerous corona sources along the length of the line and since this dissertation will study power line coronas, this review will focus mainly on corona studies utilysing test lines or test cages in air.

2.2 Hypothesis

The main hypothesis to be proved or disproved is that: *"the reduced local air density, due to the higher surface temperature of the conductor, followed by physical processes occurring on the conductor surface, is responsible for increased ionisations in the gas"*.

These local ionisation processes are interdependent and require a multi-physical model to explain their behaviour, which is outside the scope of this dissertation. Current corona models require empirical fit coefficients which describe the behaviour of the ionised gas and the processes at the conductor surface (secondary coefficient). Since these coefficients are normally obtained for cool conductors and since physical changes in the discharge phenomena (apearance of the plasma) has been observed for both polarities on heated conductors, fixed ionisation coefficients may not be valid for all cases and thereby limits the application of current corona models to cool conductors.

The next part of the review will focus on processes which influence gas breakdown to try to

establish a link between conductor temperature and these physical processes.

2.3 Theoretical basis for the Hypothesis

Early studies on gas breakdown at low pressures (typically 1 torr) have shown that the current between two electrodes will increase with the applied voltage and then reach a saturation current (remaining constant over a significant range of the applied voltage) as long as an external radiation source is present. This saturation current is dependent on the radiation intensity and can be used to measure the latter as in Geiger counters or photo-tubes (light sensors) [13]. Gas discharge studies typically use an UV-light source [11] or x-rays [13], however it can be shown that any source capable of causing electron emission from the cathode will influence this current. Electron emission will be explained in more detail later, so let us simply refer to this initial cathode current as i_0.

2.3.1 Townsends first ionisation coefficient α

Given a fixed radiation and therefore an initial supply of electrons at the rate of i_0, a further increase in the potential will lead to a sudden rise in the current, followed by gap breakdown which is often referred to as a Townsend discharge (so named after J.S. Townsend who had studied this region of the V-I curve to arrive at a basic physical model for gas breakdown). If allowed to increase, the current would reach the highest possible value and the plasma would reach a stable low impedance state referred to as an arc. This state as well as the numerous transitions of the discharge leading to an arc will not be discussed here and is well published in the literature.

According to the Townsend theorem [14], the kinetic energy attained from the field by these initial free electrons is transferred to the gas atoms or molecules during inelastic collisions. Should the amount of energy transferred be high enough to raise the bound electrons to energy levels higher than the valence band, the electrons will be freed from the atoms, leaving a positively charged ion and gaining an additional free electron which may also be accelerated by the external electric field.

As long as the conditions are favourable for ionisation, the discharge will be advanced and the number of electrons (and positive ions) liberated in a gap will increase exponentially until the anode is reached and all (negative) charges are neutralised (positive charges move to the cathode). The avalanche intensity or current as given by i in (1) is dependent on the rate of initial electrons released at the cathode, i_0, as well as the ionisation probability distribution along the gap with distance x and depending on the exponent α, referred to as "Townsend's first ionisation coefficient".

$$i = i_0 e^{\alpha x} \tag{1}$$

This coefficient α, is proportional to the average energy W_E, gained by the electrons from the electric field E, between free paths λ which can be approximated as $W_E = F_E.s = E.e.\lambda$, where e is the charge of an electron so that $\alpha = f(E\lambda)$.

The mean free path $\overline{\lambda}$ as introduced by Rudolf Clausius [15], can be shown to be inversely proportional to the molecular density or the relative gas density δ, so that:

$$\overline{\lambda}_{p,T} = \lambda_0.\frac{p_0}{p}.\frac{T}{T_0} \tag{2}$$

and therefore the ionisation coefficient $\alpha = f(\frac{E}{\delta})$ or more commonly $\alpha = f(\frac{E}{p})$ for fixed temperatures.

α in non uniform fields

Since the electric field provides the accellerating force, α can only be expected to be constant in a uniform field. At high pressures, some simplifications can be made since the mean free path is extremely small and the field will not change significantly for each flight between collitions. If dn new electrons are created from n electrons entering and traversing a slab of thickness dx, then the proportional number of new electrons created are equal to α as in (3).

$$\frac{dn}{dx} = \alpha n \tag{3}$$

if at x_1, $n = n_1$ and at x_2, $n = n_2$, then:

$$\ln \frac{n_2}{n_1} = \int_{x_1}^{x_2} \alpha dx \tag{4}$$

For the special case of a uniform field with the limits $|_0^x$

$$n_x = n_0 e^{\alpha x} \tag{5}$$

for the non-uniform field at high pressures the gain in electrons can be calculated iteratively over discrete distances using the average field and α values within the boundries $|_{x_1}^{x_2}$

$$\frac{n_2}{n_1} = e^{\int_{x_1}^{x_2} \alpha dx} \tag{6}$$

This can be further developed if the function $\alpha = f(\frac{E}{p})$ and the function of $E = f(r)$ is known, however it is outside of the scope of this work.

It has now been established that Townsends first ionisation coefficient depends on the gas density and the magnitude of the electric field. It has also been shown that the discharge current or number of charges created depends on the initial charges available at the cathode.

2.3.2 Self sustaining discharges

The discharges hitherto discussed will be transient in nature, since it requires the availability of starter electrons. If however the number of electrons can be augmented by some secondary processes, the current will increase after each transition and become stable. Such a type of self sustained discharge will cause complete breakdown in a uniform field or partial breakdown (corona) in a non-uniform field.

Townsends second ionization coefficient
Townsend had imagined the ionizing effect of the positive gas ions to be significant in achieving additional free electrons, however this was later disproved by J.J.Thomson [16] and the effect of ion bombardment at the cathode was introduced. This mechanism solved most of the problems relating to the inaccurate atomic model used by Townsend, however, as found in later studies, additional processes were needed to explain the faster than expected discharge development. These additional processes occurring at the cathode are: photo radiation, emission by metastables [17], [18] and emission by solid contaminants [19]. Even though Townsend's assumptions were wrong, the general form of his equation is almost identical to the specific solutions of all these models so that a single coefficient γ can be condensed from all the above processes and is frequently referred to as the second Townsend coefficient in honor of his work.

Breakdown
The secondary emission coefficient γ, equals the number of electrons liberated from the cathode for each colliding positive ion and since the number of ions created is equal to the number of ionizations, it can be shown that the factor of charge and current multiplication is:

$$\frac{n}{n_0} = \frac{i}{i_0} = \frac{e^{\alpha d}}{1 - \gamma_i(e^{\alpha d} - 1)} \tag{7}$$

At breakdown and for the current to increase indefinitely, the denominator must strive to zero so that the limit condition becomes:

$$\gamma(e^{\alpha d} - 1) = 1 \tag{8}$$

2.3.3 Processes in the gas

The most important processes in the gas that can yield additional electrons are: photo-ionization and electron attachment. Photo-ionization creates a second generation of electrons, especially when gases of different ionization energies are present (Penning effect), or even for same gas molecules dissociated into their atomic states. Electron attachment creates a reduction in the

amount of free electrons when electronegative gases attract some of the free electrons to form heavy negative ions, thereby reducing the ionization exponent.

2.3.4 Processes at the Cathode

It should by now be clear that both primary and secondary electron emissions influence the ionization. Primary emissions will start the process and determine the magnitude of the current reached or the charges created in a discharge and the secondary emissions will sustain the process or lead to breakdown or partial discharge (corona), but since breakdown behaviour is more interesting for this study, the processes will be explained from the perspective of secondary emissions while assuming the presence of an existing discharge.

In modern quantum physics, metals can be shown to have numerous discrete energy levels which are difficult to measure [20] and for this reason these energy states are grouped into bands according to Fermi-Dirac statistics, which describes the statistical energy states of electrons within a metal.

The electrons closest to the surface have a potential energy approaching zero. The valence electrons (of metals) in the upper levels are not bound to their parent atoms and are referred to as being in the conduction band. The energy required to remove an electron to the surface is referred to as the "work function", which is the energy gap between the highest level of the conduction band and the surface (where no work is required) [11].

Any process that can raise the energy of the electrons to overcome this gap or potential barrier will create an emission of electrons at the metal's surface; equivalently, any process that will shift the electron energy probability distribution to a higher level will reduce the energy required to remove a significant amount of electrons from the surface.

Ion Bombardment

According to classical physics, a solid surface will emit electrons when struck with ions of sufficient energy to overcome the work function of the material. This effect is of significance for the electron avalanche or breakdown since it is responsible for the supply of additional electrons [16], to sustain a Townsend type discharge.

The positive ions created during such a discharge, are accelerated back to the cathode, thereby attaining energy from the electric field, where they will release electrons from the cathode upon collision (kinetic energy is converted to potential energy). The same effect is possible when high energy electrons strike a surface (anode) as applied in photo multiplier tubes.

Even though the amount of electrons created from such collitions may be low, it creates a steady increase in the amount of starter electrons leading to an increase in the current and a stable discharge. The coefficient relating the number of electrons created for every ion

impacting the surface is γ_i. This coefficient can be lumped together with other secondary emissions coefficients and applied to equation (8) to predict breakdown.

Photoelectric emission

The photoelectric effect was discovered by Heinrich Hertz in 1887 and explained by A. Einstein [21] in 1905. The energy of a photon with frequency f can be expressed as hf where h is Plank's constant. If this energy is higher than the work function ϕ of a material, the electrons will be removed and in addition gain additional energy so that its kinetic energy is:

$$E_k = hf - \phi \tag{9}$$

Both the frequency (which determines the energy) and the intensity of the incident light will increase the current. While the current is directly proportional to the intensity of the incident light, different metals will have different sensitivity ranges for frequencies or wavelengths, so that only a certain band of frequencies will create a photoelectric effect. In fact, the effectiveness of photo-electric materials can be enhanced by special treatments especially when adding low work function alkali metals.

It is assumed that each electron avalanche creates not only ionisations α, but also a multitude excited atoms which will radiate photons toward the cathode which will cause secondary electrons to be emitted from the cathode if their energy is high enough. When considering the number of excited states, the fraction of photons that reach the cathode and the attenuation of the beam through the gas, a quantity can be derived to represent the coefficient of photo-emission γ_p which can be added to the other secondary coefficients to yield a single coefficient as used in (8).

Thermionic emission

Heating the conductor material will cause some of the electrons to attain high enough energies to leave the surface similar to evaporation as formalised by Richardson [22]

$$J = AT^2 e^{\frac{-\phi}{kT}} \tag{10}$$

where J is the current density, A is a universal thermionic constant, K is the Boltzmann constant and T the temperature in Kelvin. The effect of temperature is insignificant for pure metals at moderate temperatures.

Field emission

As mentioned before the electrons in the conduction band can be removed if sufficient energy is gained by them ($> \phi$), however it has been shown that electrons can overcome this energy gap, by tunneling through simply due to their statistical distribution. This phenomena which was first mathematically modeled by Fowler and Nordheim [23] will not be explained in detail, however it should be stated that an external field will alter the electron distribution and increase the probability of tunneling. Later derivations using these probabilities [24] showed that fields of the order of $10^9\, V/m$ are required to generate significant tunneling from simple metals, whereas significant emmission may occur in the presence of surface contaminants at lower fields, of the order of $10^7 V/m$.

Malter effect

A mechanism possibly related to the special increased field effect due to oxide layers has been identified by Malter as an augmented secondary emission effect. It is believed that oxidized particles will insulate and allow the build-up of charges very close to the cathode surface, which in turn creates fields of the order of $10^8\, V/m$ and releases high energy electrons into the gas.

Metastables

The effect of gas molecules in the metastable state has also been identified early on by [17] and Engstrom and Huxford [18]. A constant for this effect can be derived in a similar way as for photon induced secondary emissions by assuming the number of metastables produced per ionisation and then applying a geometrical function to determine the number of these metastables that would reach the cathode. This constant γ_m can be grouped with other secondary emission effects and used in (8) to predict breakdown.

Summary - Gas discharges

The process of breakdown has been presented and the dependence on the electron emissions from the cathode has been highlighted. Any of these processes that can augment the supply of electrons can therefore be expected to effect breakdown or corona inception, that is, to increase the number of charges created and raise the steady state corona current.

Aluminium, being the most common conductor material for overhead lines, has a photoelectric work function of approximately $3\, eV$ - $4.4\, eV$ whereas its most common oxide Al_2O_3, which is a good insulator, has a band gap energy of approximately $7.8\, eV$. When considering the typical measured radiation band for corona discharges in air to be between 200 nm and 850 nm [25] or 1.45 eV to 6.2 eV it seems that most of the photo-energy generated by the initial discharge would simply be absorbed by the oxide layer without contributing to a secondary emission.

On the other hand, oxide particles on the conductor surface can assist the accumulation of surface charge (ions) significantly [19] and have been shown to reduce the work function in some instances. As an example, Vanselow [26] has shown that a layer of aluminium oxide, can reduce the work function of a tungsten electrode with $\phi = 4.8\,eV$ to about $3.8\,eV$ due to changes in the barrier profile. The combined effect of the external field, an increased surface charge, a lower work function or changes to the barrier profile, the accumulation of excited gas Metastables and the build up of space charges may all contribute to higher secondary emissions as a type of field emission.

The hypothesis tries to establish a link between increased corona activity and conductor temperature, which seems probable since it has been shown that heat will increase the electron energy distribution and may influence work function measurements. Nonetheless when evaluating only the effect of conductor temperature, one finds the thermionic current to be insignificant so that it is generally not considered for "cold" plasmas. As an example, raising the temperature of a Nickel electrode from $283\,K$ to $373\,K$, will result in a current density increase of approximately 12 %; however, the current density is only approximately $2.1 \times 10^{-52}\,\mathrm{A\,m^{-2}}$ at $373\,K$ according to Richardson's equation 10)! (With $\phi = 4.6\,eV$; $A = 0.3 \times 10^6$; $K = 8.617 \times 10^{-5}$ - for Aluminium).

Even though the thermionic effect may be insignificant, the higher conductor temperature will create a reduced local air density which will not only increase the initial ionization process, but may also reduce the energy losses or attenuation of the heavy ions and light waves respectively, moving back to the cathode.

2.4 Power line corona

Corona is a phenomena encountered on high voltage conductors where the electric field intensity exceeds the ionisation threshold. The process of ionisation will dissociate the gases into their atomic constituents to recombine as corrosive gases (e.g. Ozone and Nitrous Oxide) and create free charges (electrons and gas ions). The formation and displacement of these charges in a time varying field, will lead to unwanted radio interference, audible noise and power losses.

Corona Onset

Corona onset, by definition, is the point at which a self sustaining partial discharge occurs near the conductor or line and occurs when the critical E-field or voltage gradient defined by E_c in equation 11 is exceeded. The intensity (magnitude) of the E-field has to exceed the threshold over a minimum distance; Referring to the collision model (Ionisation), to ensure that enough energy is attained from the field to ionise the gas. For non-uniform fields, in particular, the field intensity on the conductor surface has to exceed the ionisation threshold

to initiate discharges.

This equation 11 was derived by F. W. Peek [2] who had investigated the effect of relative air density, voltage and conductor configuration on corona inception using visual observations. It can be shown [3] that he probably used an analytic method similar to that of Townsend [14], but with additional empirical constants.

$$E_c = mE_0\delta(1 + \frac{K}{\sqrt{\delta r_c}}) \tag{11}$$

E_0 and K are empirical constants which depend on the applied voltage type and the conductor arrangement respectively, with δ the reletave air density, m, the rougness or "shape" factor of the conductor and r_c the conductor radius in cm. Other constants have been proposed [27] for E_0 and K, but the basic form of the equation is still in general use. Peek's equation (11) shows the critical field strength E_c to be approximately proportional to the air density δ, whereas, Peterson [28] found it to be proportional to $\delta^{2/3}$ and Robertson [29] found it to vary with $\delta^{1/2}$ when conducting tests at high altitude.

In practice, the onset gradient and the factor m (surface roughness factor) of power line conductors are determined experimentally since it depends on the conductor stranding and bundling geometry, the surface roughness of the conductor and the presence of surface contaminants.

Factors which influence corona

Based on the theoretical review of gas breakdown, it is clear that discharges are effected by many factors and can be sustained by many secondary effects or feedback mechanisms.

The primary ionisation described by the α coefficient, depends on the availability of starter electrons, the magnitude of the electric field and the mean free path length λ. In our context, this will be influenced by: the type of gas, the gas density, the conductor geometry and the applied voltage.

The secondary effects may be divided into two categories, processes in the gas and at the cathode:

Processes in the gas

- *Photo-ionisation:* the ionisation of gasses due to photons or light
- *Electron attachment:* Gases with a slight deficiency in valence electrons i.e. oxygen readily attract free electrons and are called electronegative gases. This attachment of unbound electrons to form heavier negative molecules cut off the formation of new avalanches.

Processes at the cathode

- *Ion bombardment:* The impact of heavy positive ions at the cathode will liberate additional electrons from the conductor
- *Thermionic emissions:* Electrons will be liberated from the cathode surface when heated depending on its work function
- *Photo-emission:* When the surface of the cathode is radiated by high frequency photons, electrons are liberated from its surface depending also on the work function of the material
- *Metastables:* Excited gas particles or metastables coming in close proximity to the cathode will liberate electrons from the cathode
- *Malter effect:* The accumulation of oxide particles cause a higher local field or special type of field emission

Corona modes

Corona can manifest in various forms or types and are characterised based on their physical appearance i.e. glow or filamentary -discharges. In strongly non-uniform fields or where a considerable space charge has formed, stable glow type coronas may develop, whereas filamentary or streamer discharges may develop when the field is high enough over a considerable distance.

The different types of positive and negative discharges have been studied extensively and a thorough review of earlier work may be found in [30], [10] with a thorough experimental record of its manifestations given in [12]. This work will investigate different modes of corona, but since reference may be made to certain types, a brief definition will be given below.

Anode Coronas

The first appearance of positive corona is referred to as a burst pulse, which is a faint filamentary discharge. An increase in the voltage will lead to the development of a streamer, which can be maintained and developed over some distance if the field changes steadily. A further increase in the voltage causing the build up of a steady negative space charge, may lead to a thin stable glow discharge, which is again followed by breakdown streamers. In a strongly non uniform field (e.g. thin wires) the glow may develop without being preceded by streamers [11].

Cathode coronas

For the negative polarity, unstable negative discharges, called Trichel discharges will form

first [31], followed by a more stable glow as described by Morton [32] and finally breakdown feathers.

2.5 Effect of conductor temperature

The effect of conductor current on power line corona performance has been studied early on by F.W. Peek [2] in a small corona cage using small diameter conductors (2.6 mm - 4 mm). Peek evaluated the effect of both AC and DC current flowing in the wire and used the wire temperature to calculate the air density surrounding the wire, but found this correction to be too large. A much later study in 1980 by Morgan and Morrow had found that the corona onset value for both positive and negative DC corona on smooth (coaxial) conductors was effected by conductor temperature [33]. They have derived an empirical formula for the effective temperature (12 which accounts for the temperature gradient across the corona sheath.

$$T_{eff} = T_a + 0.8(T_s - T_a) \tag{12}$$

where T_{eff} is the effective temperature, T_a the ambient temperature and T_s the conductor surface temperature.

Our initial work [4] on smooth conductors used a fixed fitting constant of $m = 0.965$ in Peek's formula while calculating the relative air density δ using the conductor temperature. Comparing the two methods reveal similar values for the critical or corona inception field strength E_c. Later work [6] using stranded conductors however yielded an adjustment factor of $m = 0.66$ proving that the same assumptions may not be made for practical conductors. All these investigations used optical or visual methods relating to the first appearance of discharges and were therefore subjective in nature. Furthermore, the first appearance of corona does not necessarily coincide with a sudden increase in power losses, i.e. some smaller discharges may prevail over a fair voltage range without a significant power loss increase for stranded conductors. This as well as the observation by Loeb, Kip and Hudson in [34], that the initial negative corona discharges or Trichel discharges are suppressed at moderate conductor temperatures, further complicates identification by visual means.

In 1990, Chartier and Stearns [1] had shown a direct correlation between conductor temperature and Radio interference- and Audible Noise- data respectively. Both quantities increased logarithmically with temperature so that a straight line was obtained when plotting the data against the log of the temperature $log_{10}(T)$, to obtain a semi-log plot with T the temperature in Fahrenheit, to avoid the number zero. Over the measured conductor temperature range from $-8\,°\mathrm{C}$ to $55\,°\mathrm{C}$, the measured quantities increased by approximately $10\,dB$.

When considering the power losses however, a difference of at least $17\,dB$ can be expected between fair-weather and foul weather conditions [35] so that fair-weather corona power losses

are deemed negligible. In fact a later study by Chartier [36] found that higher conductor temperatures reduce foul weather corona, since it inhibits the formation of water droplets.

The question may therefore be asked, why one should investigate corona effects at higher temperatures when overhead power line conductors are typically operated at temperatures not exceeding 75 °C? The answer lies in the increased need for compact lines, which require higher current densities and with it special high temperature low sag conductors. Notwithstanding the evident need for compact lines, it is still not widely adopted. As a point in case, a survey [37] conducted by the Electric Power Research Institute (EPRI), in the United States of America which included twenty respondents, has identified that "there is a lack of technical data for the design of compact lines" and have identified two topics of potential studies that could lead to wider adoption of compact lines: High-temperature low-sag (HTLS) conductors, and standard compact-line designs. Line design includes tower design, insulation coordination and conductor "arrangement" and choice. A more compact conductor arrangement increases the local field strength which is known to have a direct impact on the corona severity, however the impact of higher conductor temperatures (when using low sag conductors) is still mostly unknown.

2.6 Measurement and evaluation methods for corona

Typical nuisance factors of corona are audible noise, radio interference and power loss and it is generally assumed that all these quantities will increase as soon as corona inception occurs. Even though visual methods are satisfactory for determining the inception voltage of corona, it is not a practical means of establishing the magnitude or intensity of the individual nuisances.

The radio interference level can be measured directly (conducted EMI) or by means of an antenna to determine the noise at specific standard frequencies in $dB_{\mu V}$. Similarly, the audible noise can be measured using a microphone and a A-weighted detector to determine the sound pressure level in dB_A.

The corona power loss can be calculated from the measured voltage and current and is generally less problematic for long test lines as the individual pulses are integrated by the line. For short test lines and corona cages, the measured data has to be digitized and the power computed numerically which leads to significant errors when the sampling bandwidth is limited [7] or the current needs to be integrated which presents additional computational problems if the voltage waveshape is not a pure sinusoid.

Given the limitations with regards to the available equipment, various measurement methods were evaluated to find an appropriate technique as will be explained in the next chapter.

2.7 Summary

Even though the precise mechanism is not known, past observations, research and the known theory of gas discharges has shown there to be a link between conductor temperature and corona intensity.

The need for compact lines and the lack of knowledge regarding the corona performance of high temperature low sag conductors have been demonstrated and it has been shown that existing studies are limited to temperatures below 70 °C.

Some research evaluating audible noise and radio interference, has shown a logarithmic increase of these quantities with conductor temperature, yet no significant contributions have been made in terms of relating the expected increase in power losses.

3 Test Arrangement and test cage design

A typical corona cage design consists of two concentrically arranged conductors with the inner conductor at high voltage and the outer (cage) connected to ground. In order to evaluate power line corona at elevated temperatures, it was required to heat the conductor. One way in which this could be accomplished was to pass a current through the centre conductor using a current transformer. Since the current transformer is not rated for the full test voltage, the arrangement was inverted so that the outer conductor was at high voltage and the centre conductor was connected to ground as shown in figure 3.1. This circuit configuration allows the simultaneous control of the electric field and the conductor temperature. Additional components required for electrical measurements are not shown e.g.to determine the corona current magnitude. The test arrangement can be subdivided into four sections: The test cage, the high voltage circuit, the heating circuit and the measuring circuit.

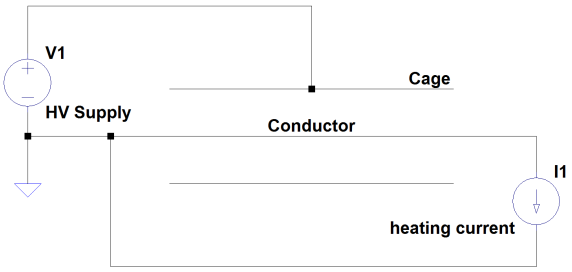

Figure 3.1: Basic circuit configuration

3.1 The test cage

The corona test cage consists of an inner conductor and a co-axially mounted outer conductor screen or cage. Using a conductor range of 10 - 25 mm and a maximum test voltage of 150 kV, the outer cage (extruded mesh) was dimensioned so that the maximum outer diameter was used that would allow a high enough E-field on the conductor to cause stable corona without flashover. The outer conductor (cage) has an inner diameter of 800 mm and is 1 250 mm long. A hoop formed of 27 mm diameter tube was welded to each end of the cage to prevent E-field concentrations at the edges. The completed test cage is shown in figure 3.2.

The outer cage was suspended with power line insulators from a support frame. The high voltage supply was connected to the cage using corona free tubes having a diameter of 40 mm. The center conductor was strung between two floor mounted posts, having insulated turnbuckles at either end to keep the conductor taught.

Figure 3.2: Corona test cage

3.2 High voltage circuit

Experiments were performed with AC using a high voltage step up transformer. The test voltage was controlled using an auto-transformer type regulator and was measured using a Tettex DMI 551 voltmeter in conjunction with a capacitive voltage divider.

The supply voltage was taken from a motor / alternator set with a sinusoidal output voltage almost free of harmonics and a 2 $M\Omega$ series resistor was placed in the secondary circuit between the transformer output and the measuring capacitor to form a low pass RC filter which further improved the voltage waveform.

3.3 Heating circuit

The centre conductor was extended to form a large loop that passed through the coaxial outer conductor or cage and the core of a current transformer. The conductor temperature was controlled by varying the primary voltage of the current injection transformer using an auto-transformer regulator and was monitored using a thermocouple attached to it 500 mm away from the cage's end. Measurements were performed to verify that the conductor temperature was stable and uniform within 2 K along the active length of the cage. The temperature of the conductor was allowed to stabilise before experiments were performed so that a change of less than 2 K occurred in 5 minutes.

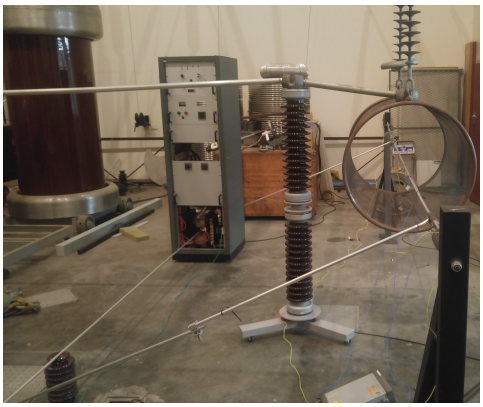

Figure 3.3: Heating arrangement

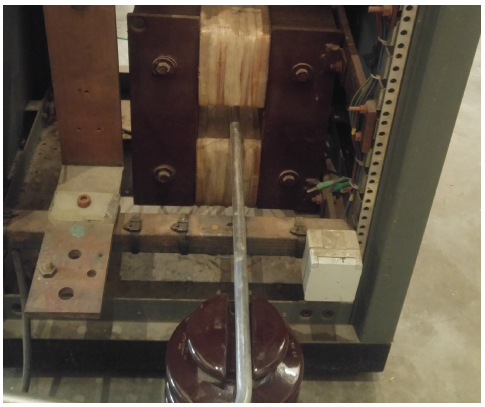

Figure 3.4: Heating transformer

3.4 Measuring circuit

In previous studies [4] results were obtained visually using a (Corocam MKI) camera with a photo intensifier which is optimised for the UV spectrum (also called an ICCD camera). Identification criteria were established to evaluate the extent of the discharges; however this was still too subjective for accurate comparisons. In an attempt to better quantify the results obtained, electrical detection techniques had to be developed for this special (inverted) case. Pulse techniques were evaluated, but due to the limited sampling speed (measurement bandwidth), a bridge technique was later adopted. In a previous study [7] which had attempted to resolve the charge per cycle using oscilloscope records, similar problems were experienced.

3.4.1 Pulse measuring techniques

Due to the high circuit inductance of the earth return and the source, a capacitor and measuring impedance was connected across the test cage to provide a low impedance current path for the corona pulses. In order to preserve the pulse shape and to reduce reflections that may be caused by improper matching, the characteristic impedance of the cage, which is essentially a transmission line, was calculated and a suitable termination or matching impedance was constructed.

with the cage length $l = 1250 \quad mm$, the cage radius $r_2 = 400 \quad mm$ and the nominal conductor radius $r_1 = 7 \quad mm$, the electrical parameters are:

$$\begin{aligned} C &= \frac{2\pi\epsilon_0 \cdot l}{ln(\frac{r_2}{r_1})} = 13.75 \quad pF/m \\ C_T &= 17.2 \quad pF \end{aligned} \tag{13}$$

$$L = \frac{\mu_0}{2\pi} ln(\frac{r_2}{r_1}) \cdot l = 809 \quad nH/m$$
$$L_T = 1.01 \quad \mu H \tag{14}$$

which yields a characteristic impedance,

$$Z_0 = \sqrt{\frac{L}{C}} = 242.5 \quad \Omega \tag{15}$$

and a wave propagation velocity,

$$v_{prop} = \frac{1}{\sqrt{L_T C_T}} = 240 \times 10^6 \quad m/s \tag{16}$$

The transition time t_t for a signal to travel from one end to the other is:

$$t_t = \frac{l}{v_{prop}} = 5.2 \quad ns \tag{17}$$

Since the Cage impedance is 243 Ω and the measuring cables 50 Ω, a simple two port impedance matching network was constructed using a 200 Ω resistor in series with a 50 Ω resistor as in figure 3.5. For calibration purposes, a matching network was connected at both ends of the corona cage using special low impedance straps as shown in figure 3.6, since significant distortions to the measured signal was observed when using simple fly-leads.

Figure 3.5:
Resistive matching termination

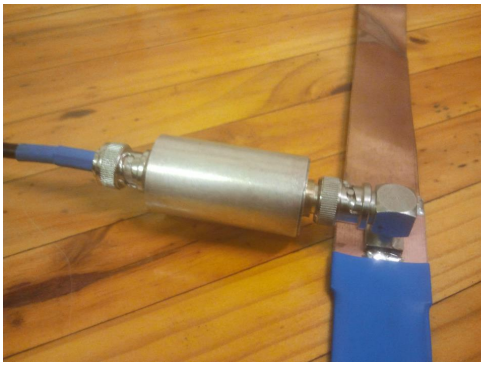

Figure 3.6:
250/50 Ω Termination

A signal was injected at the one end using a LDIC-5 commercial partial discharge calibrator or pulse generator and the system response was measured at the other end using an oscilloscope. A typical resolution time of less than 20 ns was measured for the steep fronted exponentially decaying pulse; however, when adding the high voltage coupling capacitor in series with the termination, the reproduction of the pulse shape could not be maintained due to the added series inductance, however since the integral of the measured calibration pulses with and

without the coupling capacitor differed less than 5 % from each other, the circuit was deemed acceptable.

The corona pulse currents were measured at a voltage slightly higher than corona inception using a 250 Ω resistor shunted by an inductor (to bypass most of the low frequency current). Figure 3.7 shows typical waveforms recorded at time resolutions of 2 ms, 400 μs, 1 μs and 200 ns respectively. The pulses are of short duration and in close succession, sometimes overlapping. A capture card with a high sampling rate and a deep memory is required to correctly capture the data. This is especially important when the magnitude of the pulses are to be measured accurately. In accordance with the conclusions drawn by Reid [7], it was clear that the data sampled lacked the necessary information to accurately determine the energy and / or the average power dissipated in each cycle, especially when applying filters to remove the low frequency components from the signal.

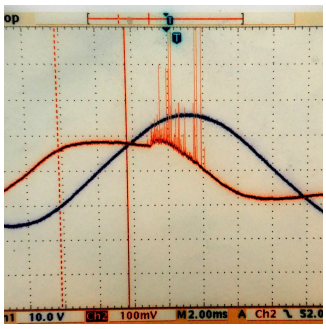

2 ms/div

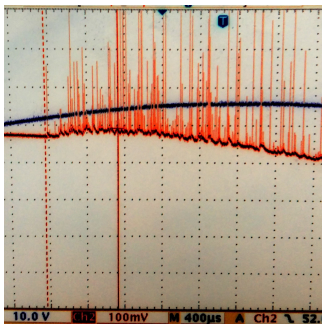

400 µs/div

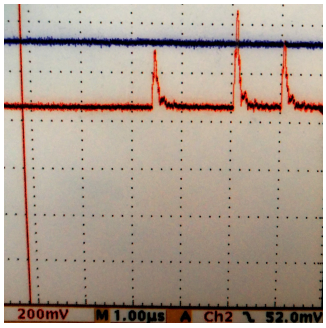

1 µs/div

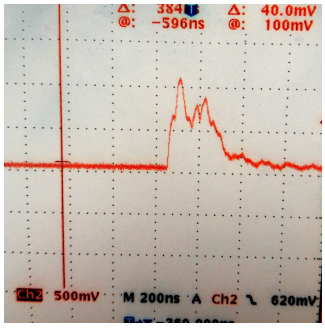

200 ns/div

Figure 3.7: Corona pulses

3.4.2 Schering bridge

Bridge circuits are used to measure component values by comparing them to known values after balancing. The losses in an insulation system, e.g. a cable, may consist of leakage currents, polarisation losses and discharges. When these losses are constant or when the discharges are small enough to be integrated or averaged out by the external circuit of the

system, they can be modeled as a fixed resistance and a bridge can be applied to measure the average losses; an example of a suitable bridge is the Schering bridge (see figure 3.8) which has been adapted in many forms to measure the losses in predominantly capacitive loads.

The standard Schering bridge was found to be inadequate for corona cage measurements as it was impossible to balance at the onset of corona discharges.

Most of the circuits based on the Schering bridge, possess a resistive element in the lower part of the sample arm. It is in part the voltage across this resistor that causes the null detector deflection. These bridges therefore have a high pass behavior and can not be balanced when sporadic pulses occur as in a small test cage. Pulse measuring techniques on the other hand and in particular partial discharge detection has been developed to evaluate the intensity of individual sporadic discharges; however, they are not suited to measure the discharge magnitude of a large number of pulses or pulses with a high recurrence as explained in the preceding section.

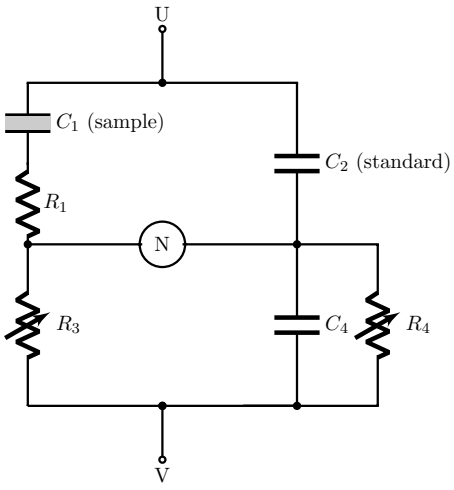

Figure 3.8: Schering Bridge

3.4.3 Standard charge integration bridge

The bridge designed by Dakin and Malinaric [38], was identified as a possible technique that could be applied. This bridge is an adaption of the charge integrator circuit of Manley [39], which is still used for dielectric barrier discharge measurements in present times.

Tests with Dielectric Loss Analyser

A commercial Dielectric loss analyser (DLA) from ERA FC-Robinson, being electrically similar to the design of Dakin, was evaluated to gauge the usefulness of the method for tests in a small corona cage.

The DLA is normally used to evaluate machine stator bar insulation and measures the corona losses in the test object by plotting the integral of the corona current (charge) against the supply voltage on an x-y display. The DLA circuit in figure 3.9 shows the built-in resistor- and capacitor decades as well as the measuring points for the vertical and horizontal voltages of the x-y display, V_x and V_y respectively; the X-axis corresponds to the voltage and the Y-axis corresponds to the charge.

The bridge is first balanced at a voltage below corona inception to compensate for, or tune out the displacement current of the sample's (geometric) capacitance until a straight line is obtained on the x-y display. The line display opens into a Rhomboid, as shown in figure 3.10, as soon as corona discharges occur in the test sample which allows the user to estimate the losses from the rhomboid area (base width times vertical height).

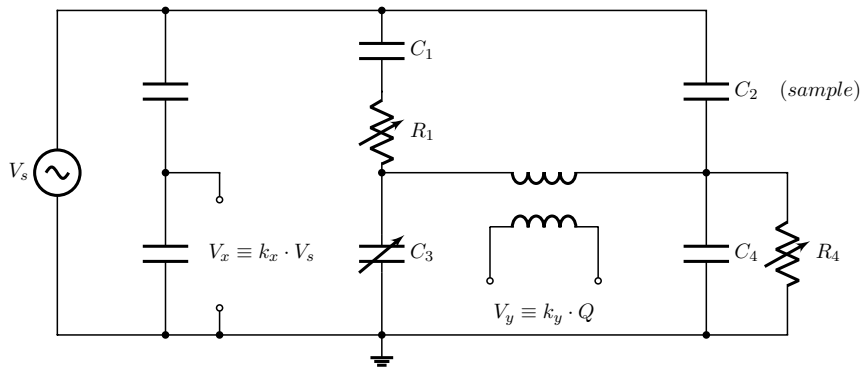

Figure 3.9: Dielectric Loss Analyser DLA - (Dakin)

Before the DLA could be used; however, some of its components were modified to allow for higher test voltages up to 150 kV as apposed to its maximum rated test voltage of 20 kV. The DLA was connected to a small corona cage and the voltage adjusted to a value below corona inception. The bridge could be balanced to straight line, but it was skewed, since the phase compensation capacitance decade lacked the range to achieve a horizontal line. After balance, the test voltage was raised until steady corona discharges were present on the test conductor, which caused the line on the x-y display to open and form a nearly elliptical trace as shown in figure 3.11 rather than a straight sided rhomboid as for stator bars (figure 3.10).

The occurrence of void discharges in stator bars with composite insulation (solid and gas), create a fairly steep and steady increase in charge on the increasing slopes of each half-cycle, after the corona inception voltage has been reached and yields a nearly straight sided rhomboid. Corona discharges; however, occur increasingly at the voltage peaks (left and right sides of the trace) and therefore the sides of the trace are more round resembling an ellipse.

A simple evaluation of the rhomboid height and width could not be used to evaluate the energy per cycle and the bridge components lacked the necessary range. The commercial

device was therefore not suited for the tests and a new bridge was constructed.

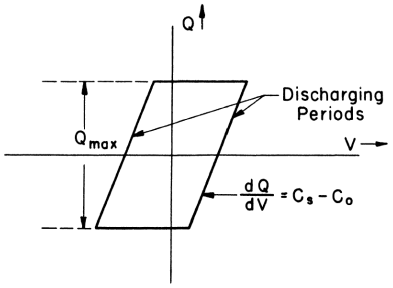

Figure 3.10:
Presumed QV-trace for stator bars

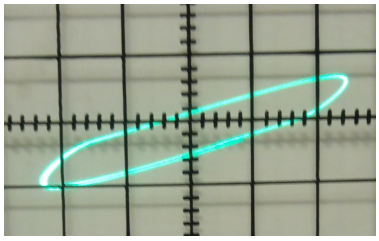

Figure 3.11:
Actual QV-trace for corona cage

Dakin bridge with extended range

A capacitance bridge with the same configuration as Dakin (DLA, figure 3.9) was constructed using a modern oscilloscope for digital data sampling and external resistance and capacitance decade boxes of sufficient range. This bridge contained a compensation resistor in both arms as this allowed for easier balancing of the bridge. A differential probe and oscilloscope was used as a null detector in stead of the transformer coupled CRT and the output from a separate voltage divider was used for obtaining the voltage data.

The bridge could be easily balanced to a straight line, which opened as soon as corona occurred. Figure 3.12 and 3.13 shows the oscilloscope records for the measurement in $Y(t)$ and $X-Y$ mode. Since power line corona manifests differently in the positive and the negative half cycle, the charge contributions were not balanced and the trace had an offset as shown. The bridge voltage signal ($Y - component$) was inverted so that a negative offset indicates an access in positive charge on the conductor (it loses more negative charges than it gains) implying higher losses for Cathodic corona (conductor negative). This led to complicated interpretation and the bridge voltage was measured to show a positive signal for an increase in positive charge on the conductor for future measurements.

3.4.4 Adapted charge integration bridge

In order to eliminate the gradual DC offset, a discharge circuit was designed, constructed and tested, that would discharge the integration capacitor at each zero crossing of the test voltage. Full details of this circuit may be found in [8] and the test arrangement of the bridge is shown in figure 3.14

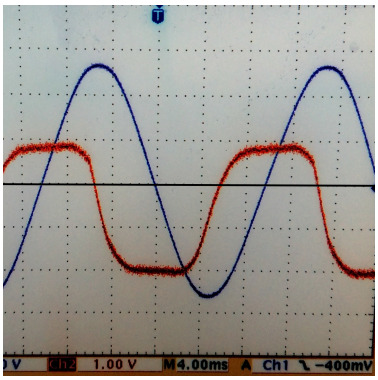

Figure 3.12:
Y(t) display for voltage and charge

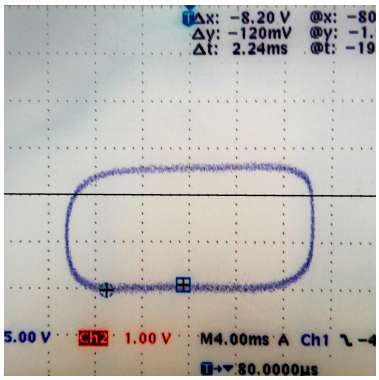

Figure 3.13:
X-Y display for voltage and charge

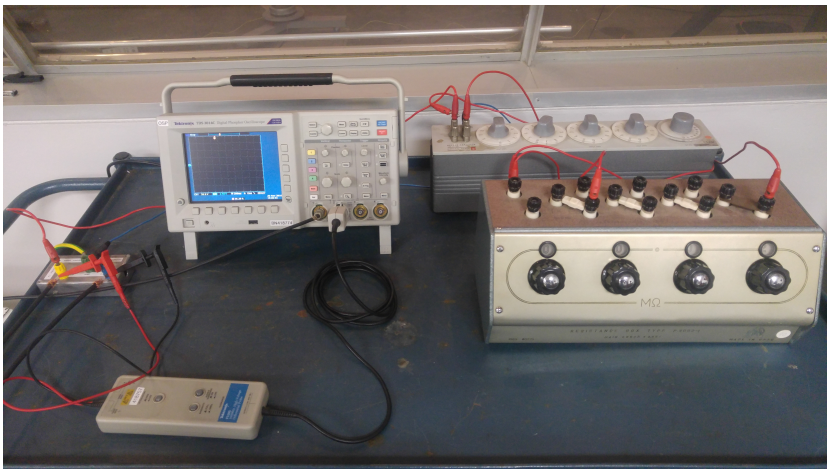

Figure 3.14: New bridge arrangement

In order to detect the zero crossings of the supply, some changes were made to the basic configuration of Dakin's capacitance bridge, especially w.r.t. the placement of the compensating resistors. It was later found that the positive and negative corona charge accumulations are more equal for tests at higher corona discharge energies, which made the charge canceling circuit unnecessary. Notwithstanding the superfluity of the charge canceling attachment, the bridge modifications had further advantages: A simpler layout, improved safety, and symmetrisation of the X-Y display.

Circuit modifications

The new circuit is shown alongside the typical circuit of Dakin in figure 3.15.

Phase compensation must be provided in order to balance the bridge. In the bridge of Dakin, phase compensation resistors are placed accross C_4 and in series with C_3.

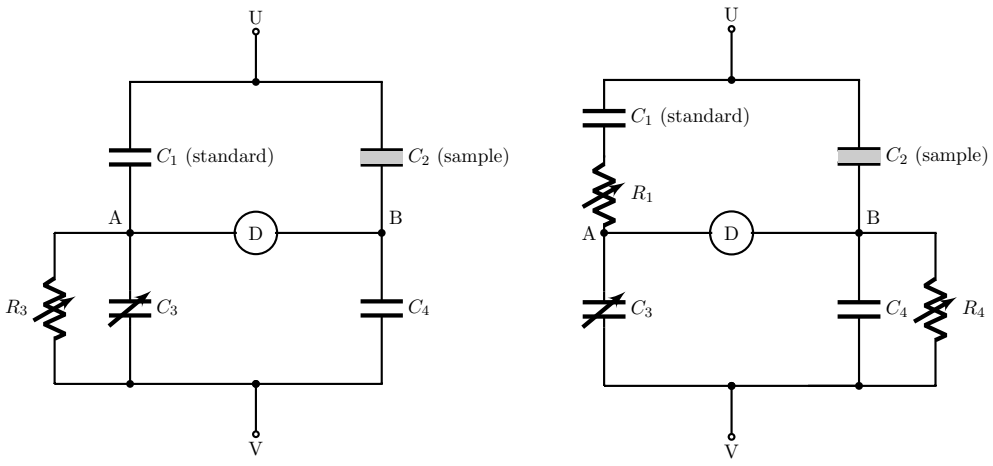

Figure 3.15:
Bridge configuration according to Pieterse (a) and Dakin (b).

The resistor R_4 effects the time constant of the charge measurement since it is placed across the integrator C_4 and the resistor R_1 in series with the high voltage divider may cause arcing or electrocution in the event of a break before make of the resistance decade. Moving the compensation resistor to the position of R_3 solves both these problems and forms a shunt compensated RC divider with the standard capacitor C_1. Since the losses in the standard arm are compensated separately, the voltage at A was now in phase with the test voltage and could be used as a reference voltage for the null detector of the charge cancelling circuit.

The voltage V for the V-Q trace is measured from a voltage divider in phase with the supply (see figure 3.9) and since the charge is measured between bridge points A and B, a phase shift in the voltage at point A (or B) will skew the V-Q trace. The phase compensation that was provided for the standard arm (R_3) had removed the phase error of the Dakin circuit and caused the V-Q trace to open symetrically when corona started.

Circuit operation

Refer to figure 3.15 (a): C_1 and C_3 together with R_3 form a voltage divider with phase compensation. C_2 is the test cage capacitance with C_4 the integrating capacitor. The supply voltage is applied accross terminals U and V and the bridge potential is measured between terminals A and B with a voltage detector D, which was realised by a differential probe and a digital storage oscilloscope.

Since the test cage C_2 has negligible losses below corona discharge inception (gas capacitor), the bridge potential at B, would be in phase with the supply voltage. Further adjustments of R_3 and C_3 will balance the bridge so that the potentials at A and B are equal.

When corona starts, the additional displacement of charge in the cage creates an increased current in the sample arm and consequently a rise in potential across C_4 which corresponds to the original corona charge Q. This additional charge raises the potential at B thereby increasing the potential difference between A and B which is measured by the detector D as $V_m = V_{AB}$.

3.5 Computation and post processing

Since the bridge voltage V_m represents the charge and since it is known that the work $W = V \cdot Q$, (with V the supply voltage), Lissajous figures or X-Y plots have been implemented in classical dielectric loss analysers to evaluate the energy loss by simple visual estimation of the area from the height and width of the pattern. The method was mainly applied to measure the losses in machine stator bars, which yields an essentially straight sided rhomboid pattern; however it is much less accurate for evaluating corona, which yields an ellipsis.

3.5.1 Lissajous figure for charge and voltage

During an experiment, the test voltage $u(t)$ and the bridge voltage $V_m(t)$ were recorded with a digital storage oscilloscope. The test voltage was measured with a voltage divider and the bridge voltage was measured using a differential probe. Matlab was used to process the digital data by applying the appropriate scaling and calculations.

After balancing the bridge, the charge was calculated from the bridge voltage V_m so that:

$$Q(t) = C_4 \cdot V_m(t) \tag{18}$$

Where:
Q =Corona charge
C_4 = Integration capacitance
V_m = Measured bridge voltage

Data arrays were created for the sampled test voltage $U = (u_1, u_2, \ldots, u_n))$ and for the charge $Q = (q_1, q_2, \ldots, q_n)$ using scalar multiplication as in 18 and were compared in an X-Y plot to produce a display as in figure 3.16.

3.5.2 Average power

The time averaged power dissipated by the sample per cycle is:

$$\overline{P} = \frac{1}{T} \int_0^T u(t) \cdot i(t) \mathrm{d}t \tag{19}$$

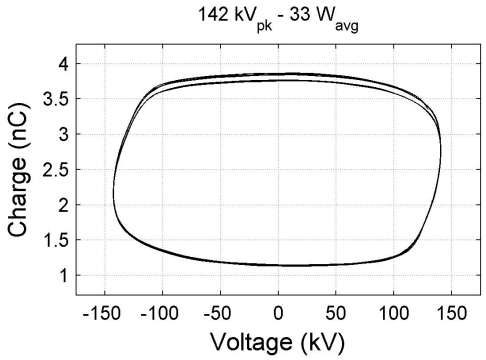

Figure 3.16: X-Y trace for charge and voltage

where:
P = Average power
T = Period of wave
u = Instantaneous voltage
i = Instantaneous current

The current; however, is not known, but can be derived from the charge in (18) so that:

$$i(t) = \frac{\mathrm{d}}{\mathrm{d}t}Q(t) = C_4\frac{dV_m}{dt} \tag{20}$$

Substituting (20) into (19) yields:

$$\overline{P} = \frac{1}{T}\int_0^T u(t)\cdot C_4\cdot \mathrm{d}V_m = \frac{1}{T}\oint_C u(t)\cdot \mathrm{d}Q \tag{21}$$

which proves that the area under the curve C, represents the work per cycle. The area was calculated in Matlab using the trapezoidal method as well as Gauss's area formula (also known as the shoelace or surveyor's formula) by implementing the built-in Matlab functions `W=Trapz(V,Q)` and `W=polyarea(V,Q)` respectively, where W represents the total work, V the test voltage and Q the corona charge.(The data captured stretched over a few cycles)

The energy per cycle and the power is then:

$$\begin{aligned} W_{cycle} &= \frac{W}{n_{cycles}} \\ \overline{P} &= \frac{W_{cycle}}{T_{cycle}} \end{aligned} \tag{22}$$

Where:

W_{cycle} = Energy per cycle
W_{total} = Total energy
n_{cycles} = Number of cycles traced
P_{avg} = Average power
T_{cycle} = Period of the cycle

3.5.3 Current and instantaneous power

Since the sampling time or interval dt is known, the current could be calculated from the time derivative of the charge as in (20) to create a data array for the calculated current. In Matlab, the gradient was obtained over each time interval for the data series Q e.g. `i = gradient(Q,dt)` to provide data for plotting . In addition, the instantaneous power was calculated from $P(t) = u(t) \cdot i(t)$ and the average power was obtained numerically from array multiplication of the voltage and current data as shown in (23) to provide a check for the power value calculated otherwise. As expected, all the integration methods yielded the same result up to four significant places.

$$P = u \cdot i = \frac{1}{n} \sum_{k=1}^{n} u \cdot i = \frac{1}{n}(u_1 i_1 + u_2 i_2 + \ldots + u_n i_n) \tag{23}$$

Figure 3.17 shows a typical supply voltage waveform ($145kV_p$), figure 3.18 the calculated charge and corona current and figure 3.19 the instantaneous power.

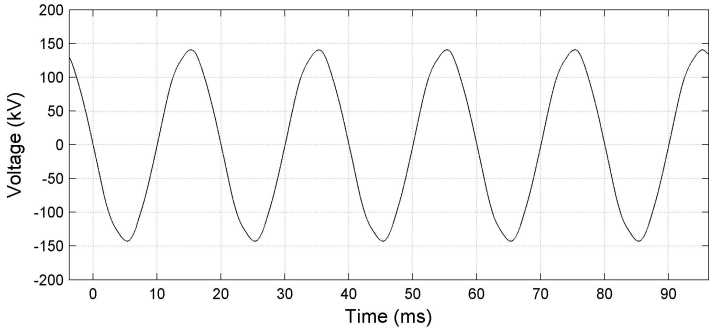

Figure 3.17: Applied Voltage

In figure 3.19 the positive supply half-cycles are shown in red and the negative half-cycles are shown in blue. Since the cage was "inverted", the conductor was always at the opposite polarity and therefore the values referred to as "positive" and "negative" refer to the Cathode and Anode coronas respectively.

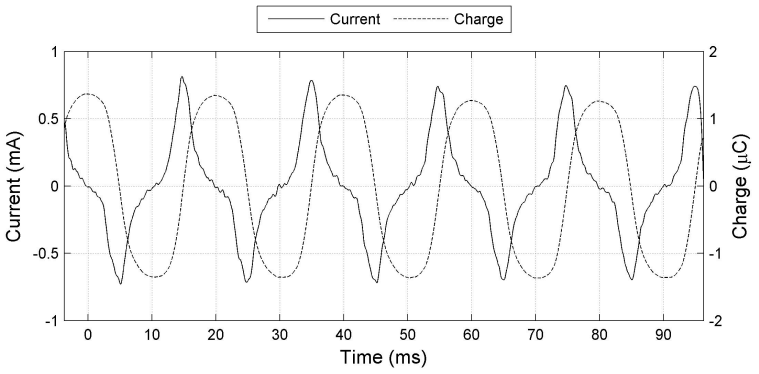

Figure 3.18: Charge and derived current

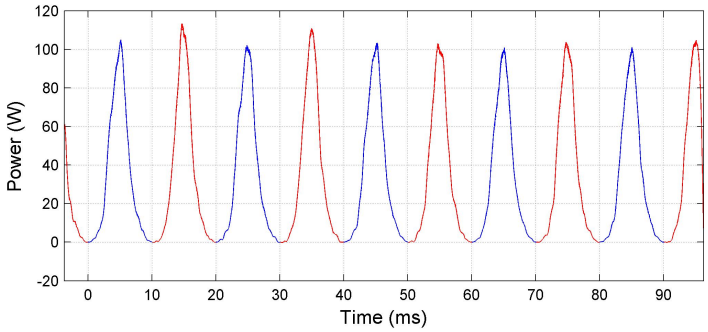

Figure 3.19: Instantaneous power

Energy and power over half cycles

Since it was found that an imbalance occurs w.r.t. the amount of charge accumulated over the positive and negative half cycle, it was decided to evaluate the two half cycles independently.

The data array for the voltage was modified to contain only positive, or only negative data points. With the remaining (oposite) values returned to zero. Data obtained from the initial bridge circuit 3.14 was evaluated. Using the modified data, separate polygons are formed as shown in figure 3.20 and 3.21 for the negative and positive voltage arrays respectively.

A computation is performed to calculate the area enclosed by the polygons and in this way the energy per half-cycle could be evaluated seperately using the `polyarea(V,Q)` command. Part of the computation script in Matlab© is shown below.

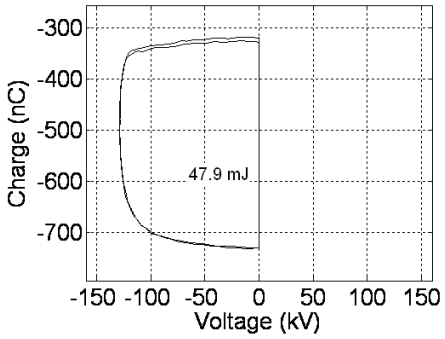

Figure 3.20: QV trace - negative

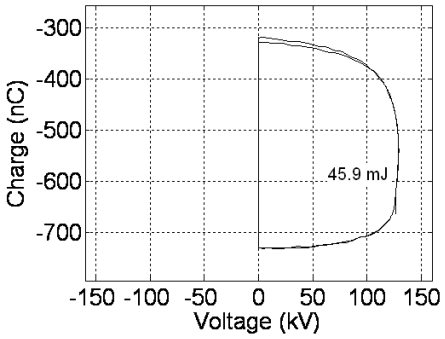

Figure 3.21: QV curve - positive

```
%Calculation of Work / Energy in Joules
cycles=(r*dx/0.02);                                  %number of cycles with T=0.02
pos=V>0;                                             %create boolean vector 1 / 0
Vpos=V.*pos;                                         %new vector for positive voltages
neg=V<0;
Vneg=V.*neg;                                         %new vector for negative voltages
Wt=round((polyarea(V,Q)/cycles)*10000)/10;           % Total Joules / cycle
Wp=round((polyarea(Vpos,Q)/cycles)*10000)/10;        % Positive cycle Joules
Wn=round((polyarea(Vneg,Q)/cycles)*10000)/10;        % Negative cycle Joules
% Answers in mJ rounded to 1 decimal place
```

Where:

r = number of intervals / samples

dx = sample interval in seconds

V = data vector for voltage

As the data usually contains more than one cycle, this method determines the average Joules / cycle. The algebraic sum of the average negative and positive energy equals that calculated for the full cycle.

Even though the charge per cycle could be measured and the positive and negative half cycle energies separated, the DC offset proved to limit the measurement range or sensitivity, especially at low corona conditions. A novel reset circuit was designed, built and tested to eliminate the DC offset and evaluate the usefullness of such a circuit.

Charge cancelling circuit

Figure 3.22 below shows a block diagram of the zero detector circuit with charge canceling means and the associated bridge connections.

The charge canceling circuit senses the voltage of the test supply using a capacitive attenuator essentially forming part of C_3. This voltage is buffered using a high impedance amplifier and squared off. Using two mono-stable multi-vibrators as edge detectors, a short output pulse

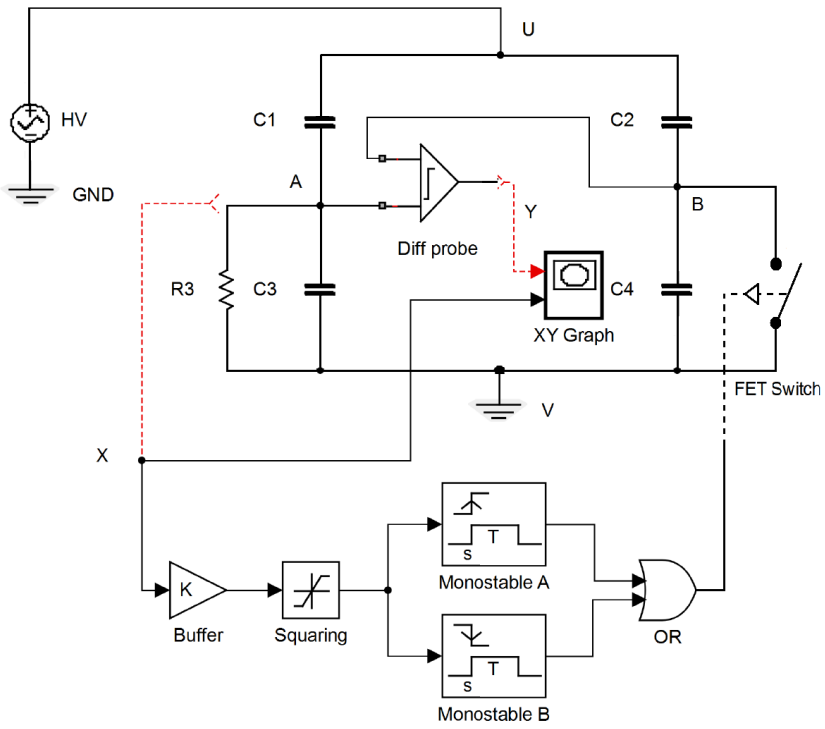

Figure 3.22: Test arrangement with discharge circuit

is generated at each state transition. These pulses are fed to an insulated gate driver, which forward biases two back to back FETs which are connected across the capacitor C_4. This effectively short-circuits C_4 in the specimen arm at the zero crossing of the supply voltage. A slight unbalance is created, however if the discharging pulse time is kept small, the offset error is minimal.

Figure 3.23 shows the bridge arrangement as set up for measurements in the control room.

Initial results with Charge cancelling circuit

Using the same cage geometry and conductor, the voltage was again raised until the corona discharges had stabilised. The discharge circuit was switched on and the trace of figure 3.24 was obtained. It is clear from these results that the pattern is now centred on the 0V line, distortions however occur due to the disruption of the balance condition.

Similarly to the method explained before, The positive, negative and full cycle energies were calculated using Matlab and are shown diagramatically in figures 3.25 and 3.26. These results are at low corona activity and therefore the distortion at the zero crossings are more significant.

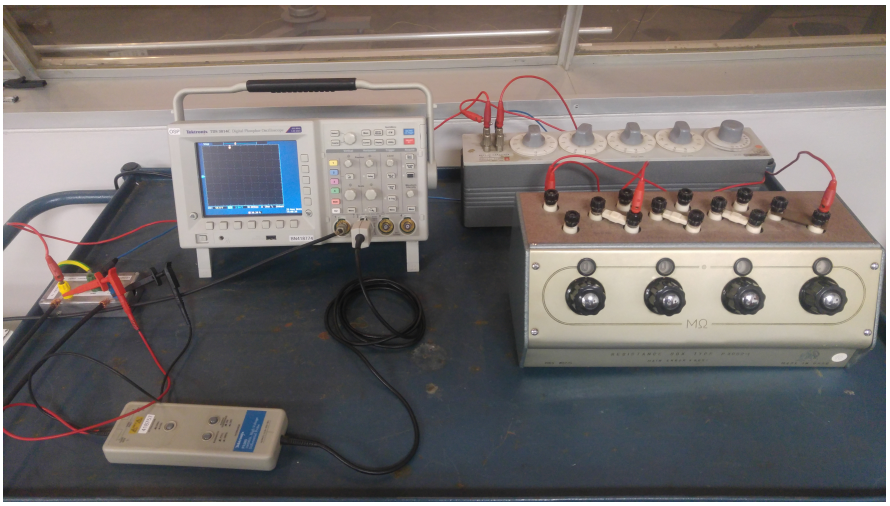

Figure 3.23: Test bridge arrangement

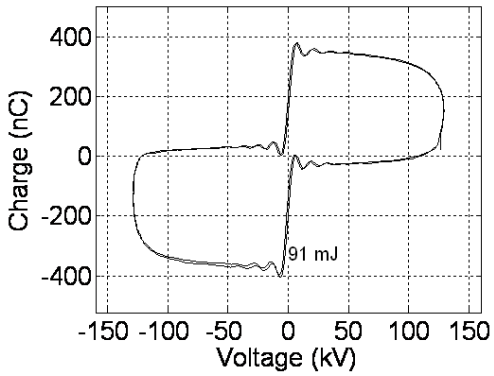

Figure 3.24: QV trace with zero circuit

As before, the sum of the positive and negative half-cycles equals that of the full trace. The symmetry of these distortions effectively cancels their effect on the trace area or energy computation. Even though the positive and negative corona charge contribution can be assessed, a method was devised to remove the distorted data values near the zero crossings (during discharge operation). More information about this can be found in [8].

3.6 Calibration of measuring circuit

The two main test quantities are the Test Voltage and the Equivalent Charge. The voltage calibration was performed using a laboratory standard divider to compare the measured value with the actual value to find the calibration ratio. The charge calibration of the test circuit was done by charge injection.

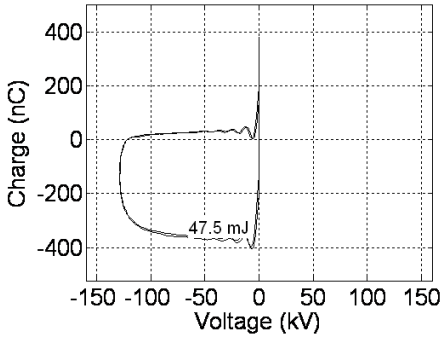

Figure 3.25: QV trace negative half-cycle

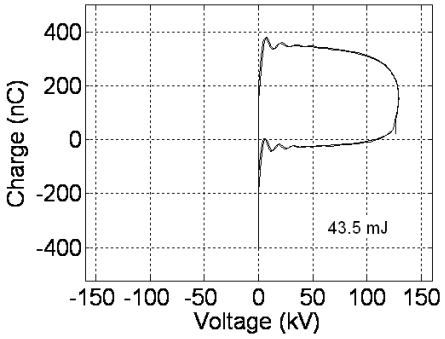

Figure 3.26: QV curve - positive

3.6.1 Charge injection test

Initially it was attempted to use a Partial discharge calibrator with a maximum signal of 500 pC. This test however, showed a nearly unnoticeable change in the bridge voltage ($Q =$ 500 pC / 100 $nF = 5\ mV$). The circuit sensitivity is determined by the integrating capacitor C_4 which is currently 100 nF and since earlier tests revealed charge magnitudes up to 820 nC, it was deemed that calibration pulse of $> 1\ nC$ was required (rather than increasing the circuit sensitivity).

The built in charge injection calibrator of a Robinson ERA discharge detector was used as it utilises a Klystron (gas discharge tube) driven high voltage pulse generator. Using a higher voltage pulse reduces the required injection capacitance for the same charge, which if kept much lower than the bridge capacitance, would dominate the total series capacitance and hence simplify the charge calibration to $Q_{injected} = C_{series} * V_{signal}$.

During calibration, a signal of 104.3 V was injected via a series injection capacitance of $100pF$ which yielded an injected charge magnitude of 10.43 nC. A signal of 105.2 mV was measured, requiring a scaling factor of 0.991 to be used. It was however considered that an uncertainty of < 1 % was acceptable.

4 Results

This chapter will present the main results for the work and show the results for corona inception, the appearance of the discharges as well as the development of the electrical current, charge and power for increased conductor temperatures.

The imaging results were not intended as a quantitative measurement, but only to support the measured electrical results e.g. corona losses, which was the main focus of the work. Quantitative measurements of light intensity require the use of a calibrated lens and detector and consideration of the effects of the gas between the object and the detector, so that an estimation of the radiated energy in the plasma can be made. In addition, the observation should be made on at least two axes and only represents the energy dissipated in the plasma during the creation of free charges. The work done on these invisible charges by the external field, can only be determind from the current.

4.1 Corona onset

A camera with an image intensifier was used to evaluate the relationship between the conductor temperature and the onset of ionisation (which is associated with light emmission).

A Corocam Mark I image intensified or ICCD camera (intensified charge coupled detector) was used to determine the onset of corona for various conductor temperatures in a darkened room. The inception point was determined subjectively and corona inception was defined as the point at which more than one corona discharge site appeared so as to exclude the effects of local surface deformations i.e. small burrs or dust particles. The image intensifier gain was set to maximum and the lens shutter (UV 105 f/4.5) was fully open to obtain the maximum sensitivity. The conductor was cleaned with fine steel wool (grade 00) and wiped clean with isopropanol or isopropyl alcohol (propan-2-ol) before each experiment, the temperature was raised in steps and allowed to stabilise before recording the corona inception voltage for each step. Figure 4.1 shows the corona inception as a function of conductor temperature in the range of 14 °C - 140 °C. As the temperature was increased, the inception voltage decreased initially, but started to increase again after 40 °C settling of at temperatures above 115 °C. The suppression of the observed corona at 40 °C is supported by the findings in [34].

At temperatures below 40 °C, the observed corona at inception, was predominantly negative (cathodic) trichel corona which appeared as many randomly spaced stationary spots on the conductor. The number of onset sites or spots reduced with an increase in conductor temperature and a positive or anode glow region with increasing size and intensity was formed around each cathode spot (negative corona tuft) as shown in figure 4.2 for 140 °C. The negative discharges were more intense than at temperatures below 40 °C, and were unstable in appearance and position.

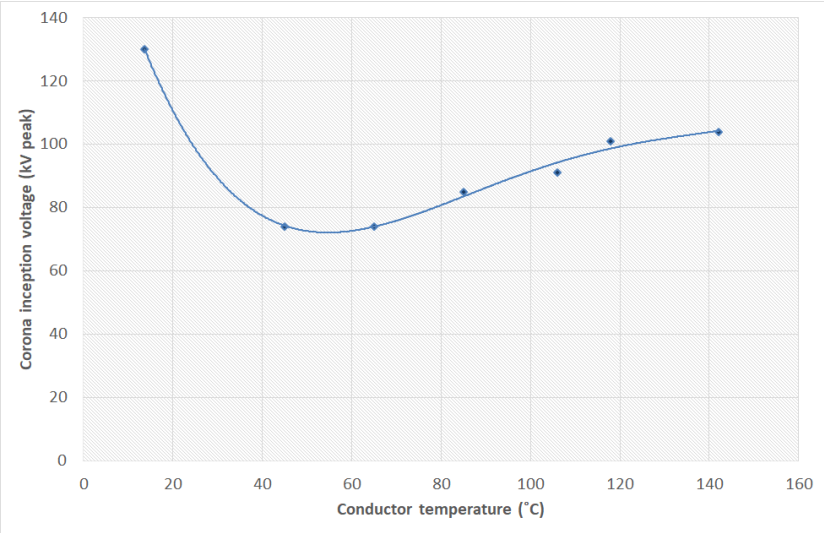

Figure 4.1: Corona inception voltage using ICCD camera

4.2 Corona luminous intensity

The relative luminous intensity of the corona discharges was evaluated using the same camera and lens to evaluate the corona modes and to observe the general discharge behavior. The luminous intensity was observed to be higher for both higher voltages and higher temperatures. Figure 4.2 shows the relative intensity of corona discharges for a conductor at 140 °C using a high gain setting on the camera. Even though some features are hidden by the overexposed image obtained, the discharges are visibly more intense at higher voltages.

A second set of images at a lower gain setting (figure 4.3) provided better detail for the bright cathodic discharges, but hid some of the anode glow regions. Compare the images for 130 kV at high and low camera gain settings in figures 4.2 and 4.3 respectively.

4.3 Electrical measurements

Since the luminous intensity is difficult to measure, electrical methods were used to determine the corona intensity.

The main objective of the experiments was to establish the general behavior of corona losses as a function of the conductor voltage and temperature, however other interesting observations were made in the process with regards to the waveforms and will be presented too. The complete set of graphs may be found in the Appendix, however for brevity this section will only give the most relevant results.

4.3.1 Test method

The test sequence consisted of the following steps:

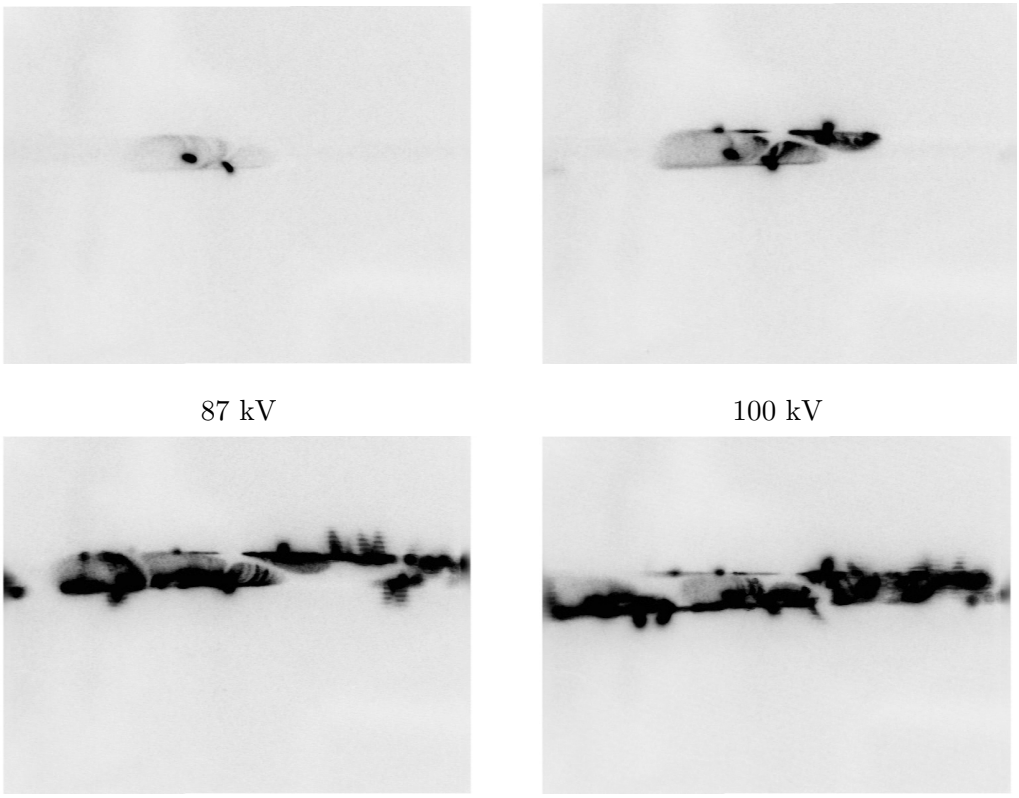

87 kV 100 kV

120 kV 130 kV

Figure 4.2: Corona images at (140 °C)

- Clean the conductor
- Set the heating current
- Wait for stable temperature (equilibrium)
- Test for a regular temperature distribution
- Balance the bridge at a voltage below inception
- Conduct corona loss measurements at various voltage steps
- Switch off, set the next heating current and repeat

The practical range of test temperatures was between 14 °C and 140 °C. The test voltage range; however, had to be restricted to the flash-over voltage of the test cage as this may have damaged the test circuit. Details on the heating circuit and the limits for equilibrium can be found in chapter 3.

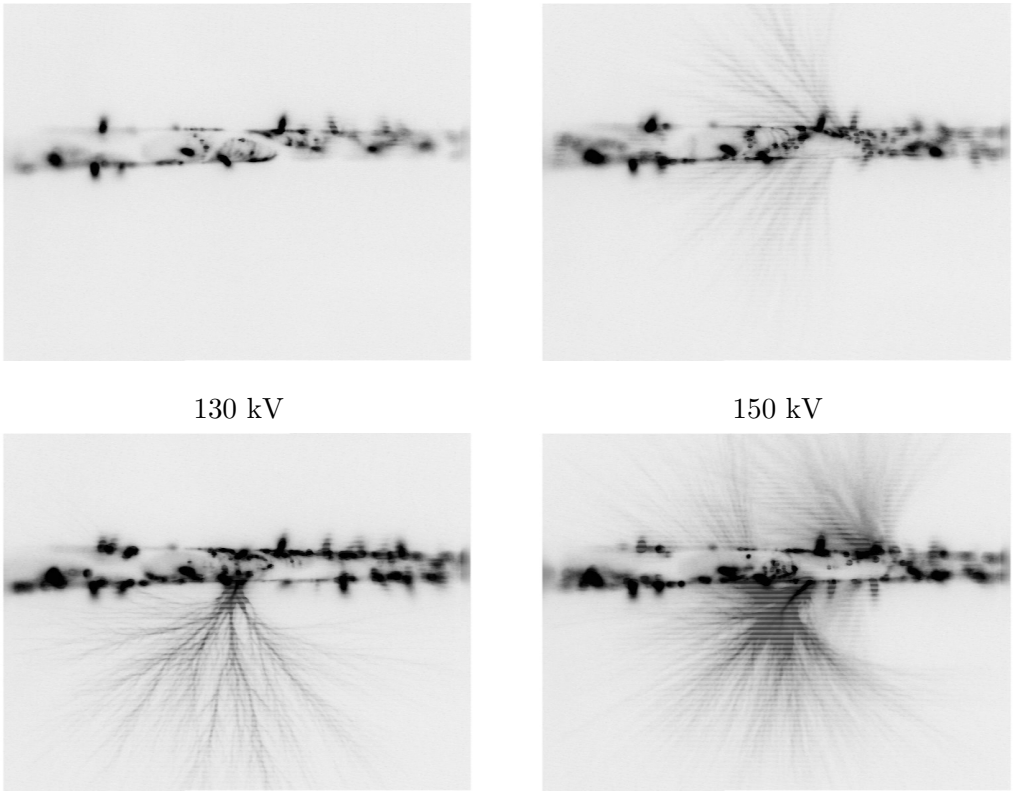

130 kV 150 kV

165 kV (1) 165 kV (2)

Figure 4.3: Low gain corona images at (140 °C)

4.3.2 Test voltage, charge and current

For each test iteration, the test voltage and corona charge was measured using digital sampling and all other quantities were calculated as explained in chapter 3. A digital, second order, Butterworth filter was applied to smooth out the wave or to remove the sampling noise. The sampling frequency was 100 kHz and the cutoff frequency of the filter was set to 1 kHz.

The test voltage was sinusoidal with low harmonic distortion. As explained in section 3, this was achieved by using a motor-generator set and RC filtering.

The corona charge is proportional to the capacitance value of the capacitor C_4 and the bridge voltage V_m (see (18)) and was calculated using scalar multiplication. The average current over each sampling interval was obtained from the gradient of the charge.

Fig 4.4 (a) shows a typical test voltage waveform along with the measured charge and derived current (b). The DC offset of the charge waveform was removed for all further time based and X-Y displays or Lissajous figures for simpler comparison.

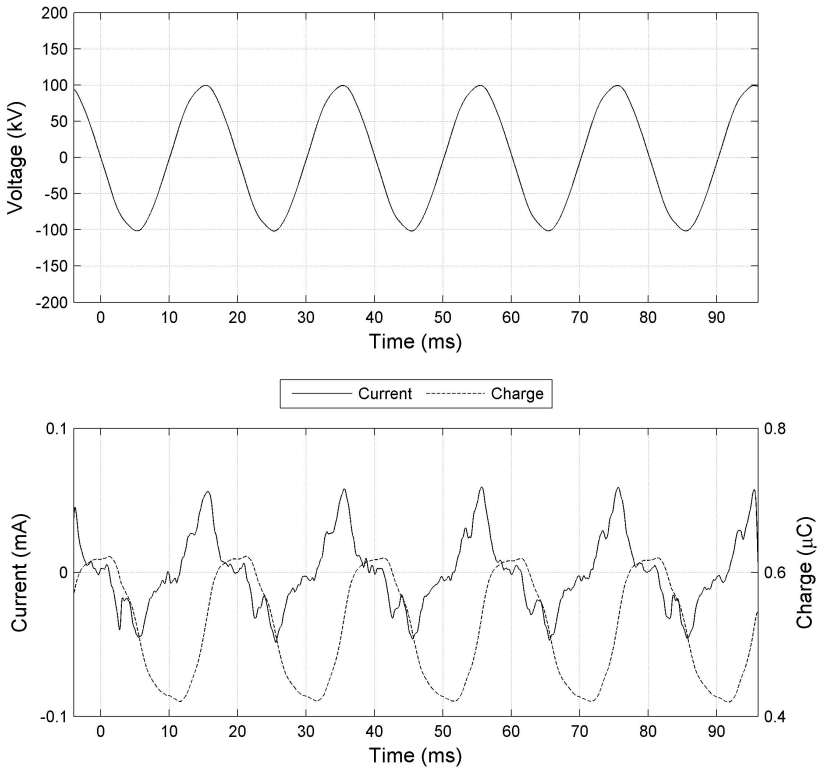

Figure 4.4:
Typical waveforms for the test voltage and corona current and charge with offset

4.3.3 Evolution of current and instantaneous power for different temperatures

As stated, the average current over each sampling interval was computed from the measured charge. The waveforms shown are therefore not the true current waveform, but relates to the integral of the current over each sampling interval (only $Q = \int idt$ is measured).

The instantaneous power was calculated from the voltage and current data arrays and is therefore also proportional to the instantaneous charge. Both the waveforms for current and instantaneous power are presented to allow for a simpler interpretation of the resulting waveforms. Sporadic or rough waveforms represent unstable corona and smooth waves represent stable corona (comprised of regularly spaced pulses).

The current and power waveforms are grouped according to conductor temperature. Three temperature cases are shown to represent low medium and high temperatures from the test range. For each of these groups the data is shown for three voltage levels corresponding to a low, medium and high value. These values were chosen arbitrarily to represent a case shortly after corona inception and two further voltages up to the highest test voltage. Note that corona inception differed for the three cases as shown in figure 4.1

Figure 4.5 and 4.6 shows the current and the power waveforms respectively for 14 °C, Figure 4.7 and 4.8 shows the current and the power waveforms respectively for 65 °C and figure 4.9 and 4.10 shows the current and the power waveforms respectively for 140 °C. The positive half-cycle values for the power were coloured red and the negative half-cycle values blue.

The current and power waveforms remain more or less constant in shape, having its peaks close to the voltage peaks where the field is at its maximum. At higher voltages the current and peak power increases and the peaks widen (The corona starts earlier on the wave). At still higher voltages the current and power is less smooth. In the range of temperatures where the corona inception is at its lowest e.g. 65 °C, the current and power at the onset of corona is very sporadic or unstable.

4.3.4 Evolution of the average power for different temperatures

Plotting the charge and the voltage on an X-Y scale provided a useful Lissajous figure display during measurements so that the inception voltage and the relative magnitude of the corona could be estimated. At inception the display is erratic and the shape is not well defined as shown in figure 4.11. At larger voltages; however, the corona and the display stabilises as shown in in figure 4.12; the stacked line trace obtained shows the data over a few cycles and is caused by deviations in the discharges for consecutive cycles. Figure 4.13 shows a typical development of the Lissajous figures for increasing test voltages at a temperature of 45 °C.The peak value of the test voltage and the average power (calculated over the complete sample) is shown directly above each trace. For further comparison, only the values were considered.

4.4 Effect of voltage on the measured charge

Figure 4.14 shows the relationship between the test voltage and the peak to peak corona charge for different conductor temperatures. The peak to peak charge is the charge created and/or displaced in one half-cycle or the maximum change in charge over a full cycle.

The charge increases almost linearly as the voltage is increased and is higher for higher conductor temperatures. The take off point for each data series occurs at a lower voltage for hotter conductors and the effect of temperature is less significant, if at all, for conductor temperatures above 100 °C. At higher voltages, breakdown occurs since the charge and current is high enough to sustain breakdown.

4.5 Effect of voltage on the total power

Since the charge is proportional to the supply voltage, the power will be proportional to the square of the voltage. The Power as a function of the voltage is shown in figure 4.15 and the quadratic relationship can be clearly shown.

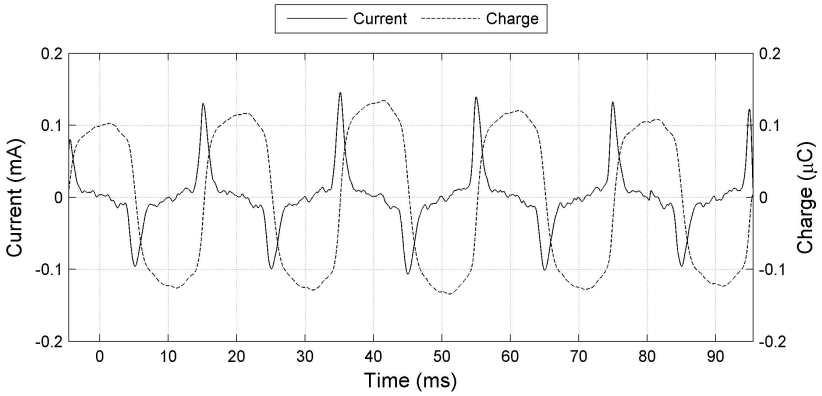

128 kV

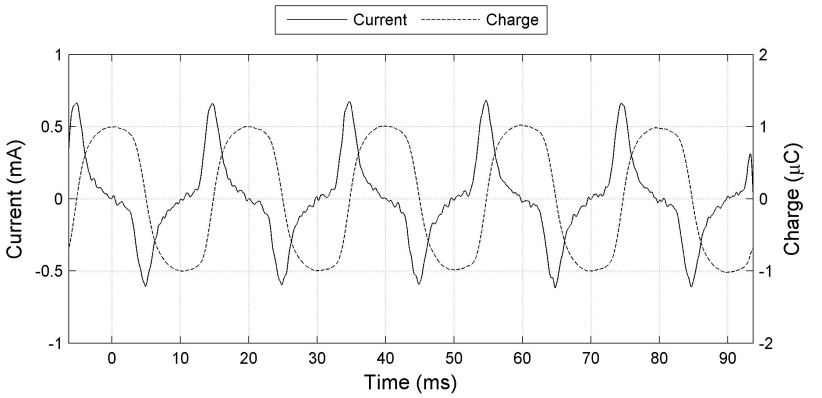

143 kV

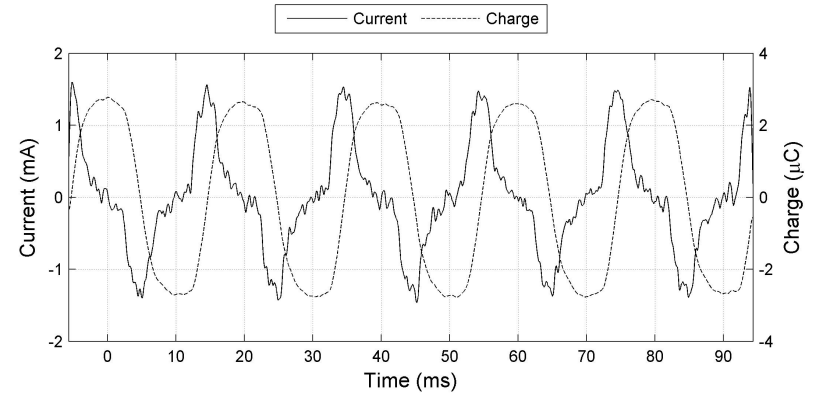

167 kV

Figure 4.5: Current development at different voltages for 14 °C

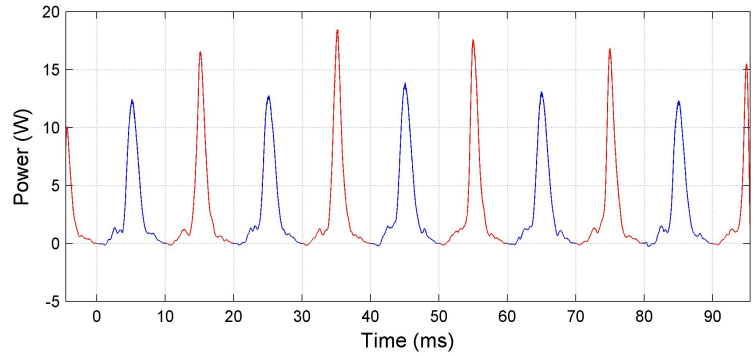

128 kV

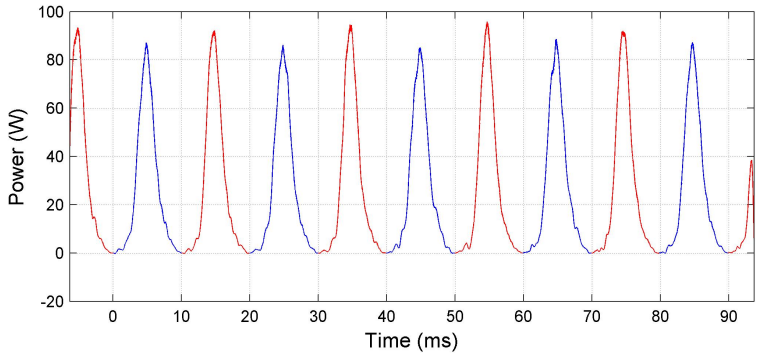

143 kV

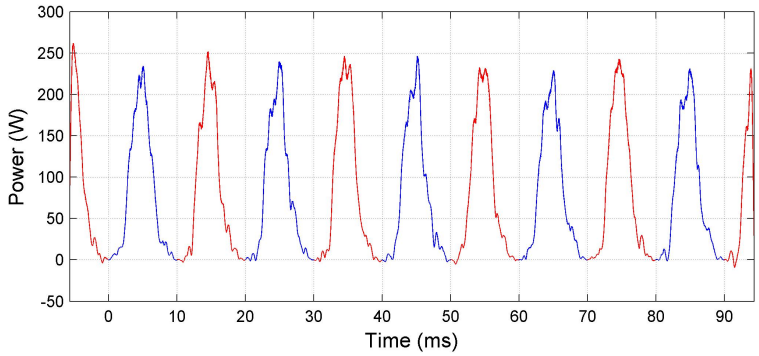

167 kV

Figure 4.6: Instantaneous power development at different voltages for 14 °C

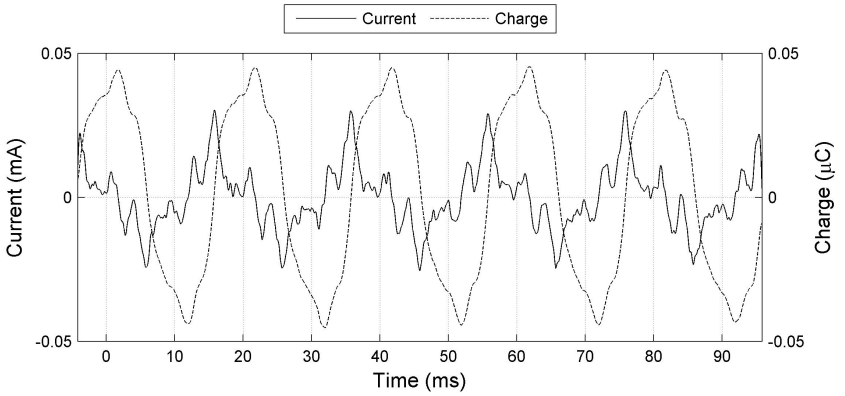

88 kV

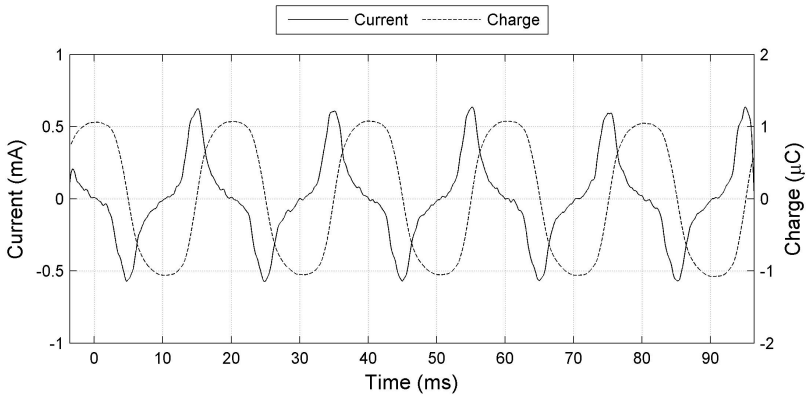

135 kV

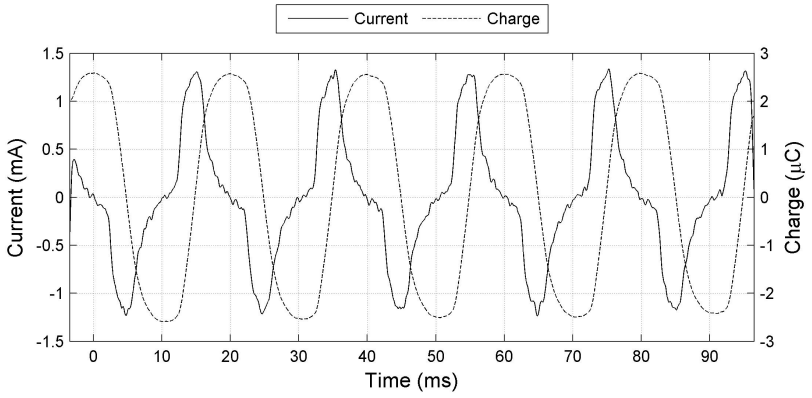

158 kV

Figure 4.7: Current development at different voltages for 65 °C

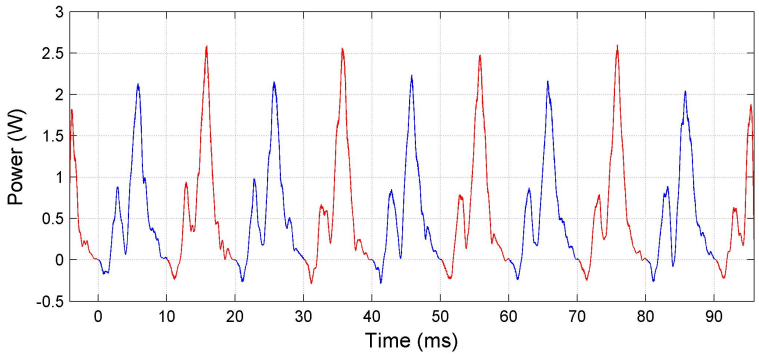

88 kV

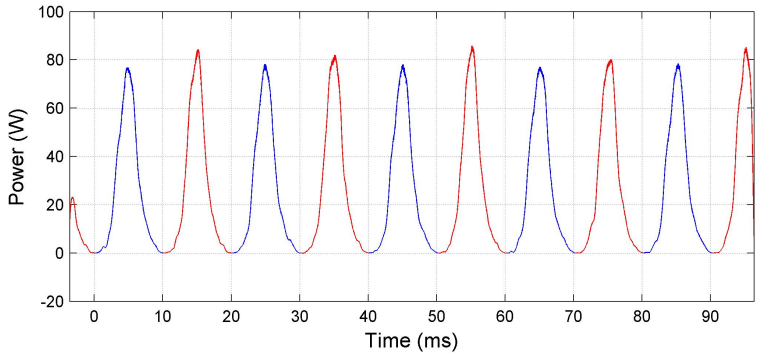

135 kV

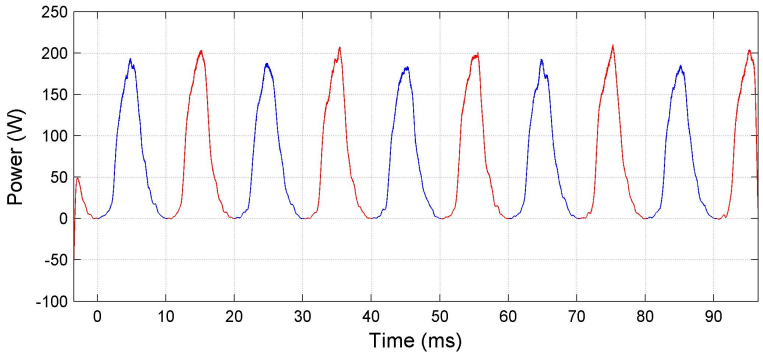

158 kV

Figure 4.8: Instantaneous power development at different voltages for 65 °C

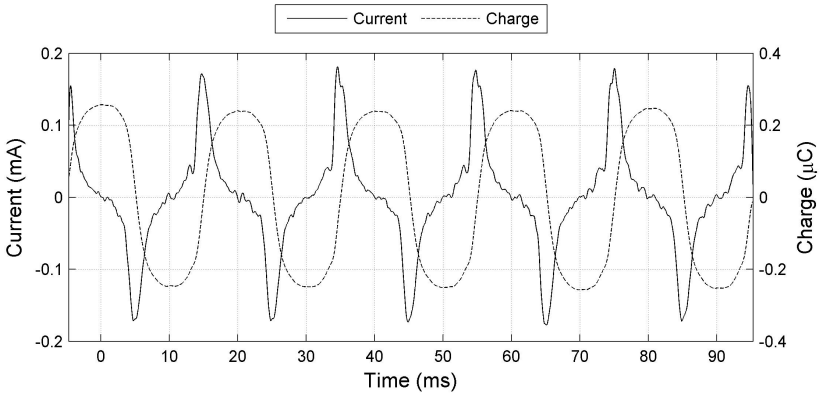

107 kV

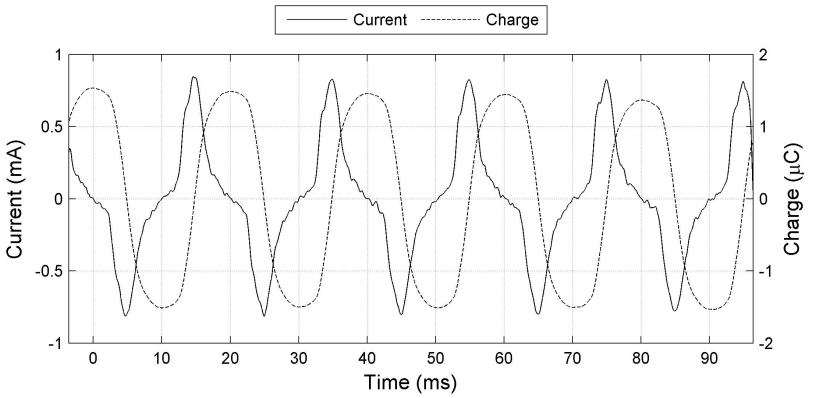

135 kV

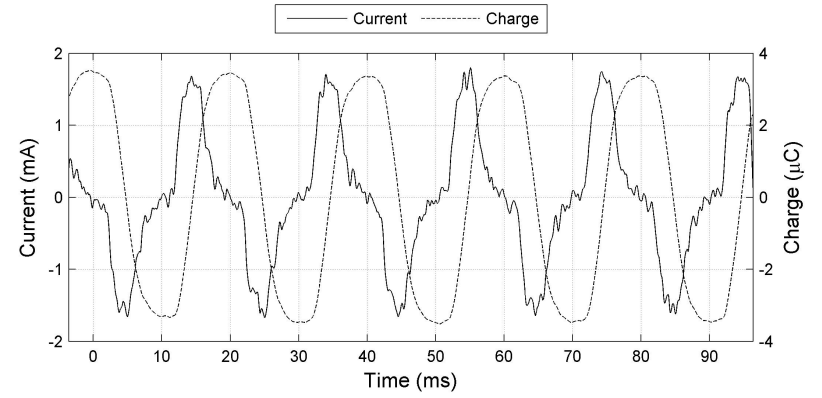

166 kV

Figure 4.9: Current development at different voltages for 140 °C

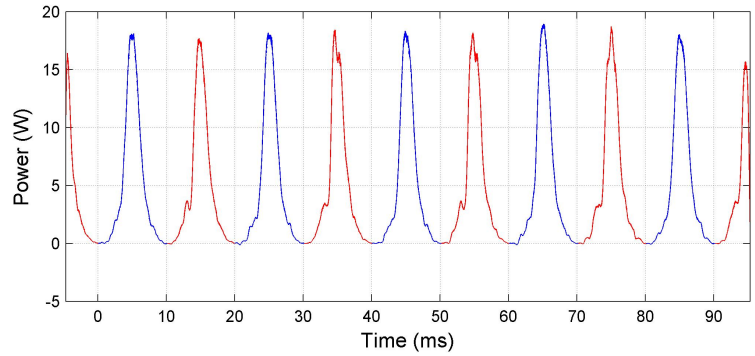

107 kV

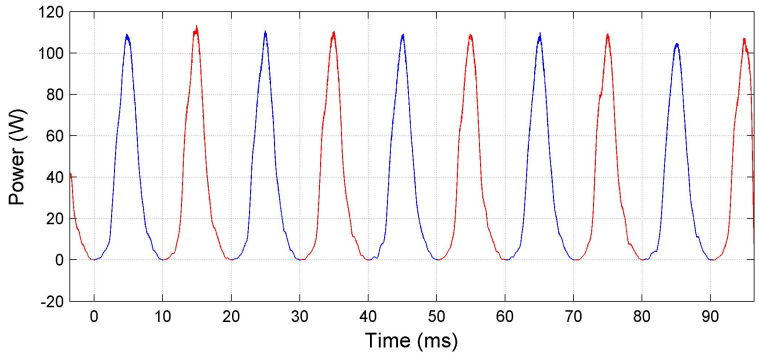

135 kV

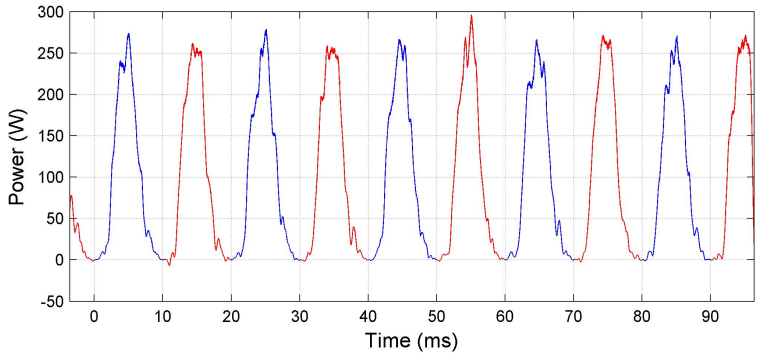

166 kV

Figure 4.10: Instantaneous power development at different voltages for 140 °C

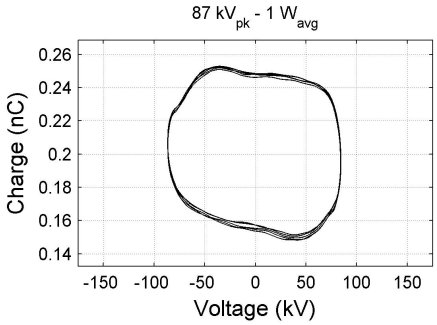

Figure 4.11:
QV-trace at inception (45 °C)

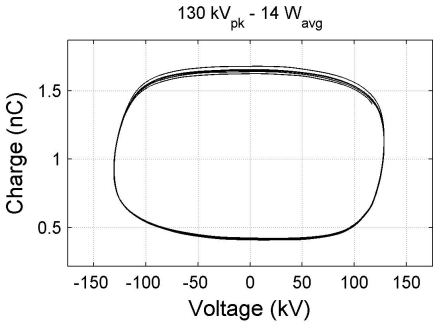

Figure 4.12:
Stable QV-trace (45 °C)

4.6 Effect of temperature on power loss

To evaluate the effect of temperature only, the power was compared to the temperature for different voltages in figure 4.15. The stacked lines are spaced in the horizontal direction in accordance with the quadratic power increase for increasing x-values or voltage as in figure 4.16.

It is interresting to note that the power increase as a function of temperature is fairly linear having similar slopes.

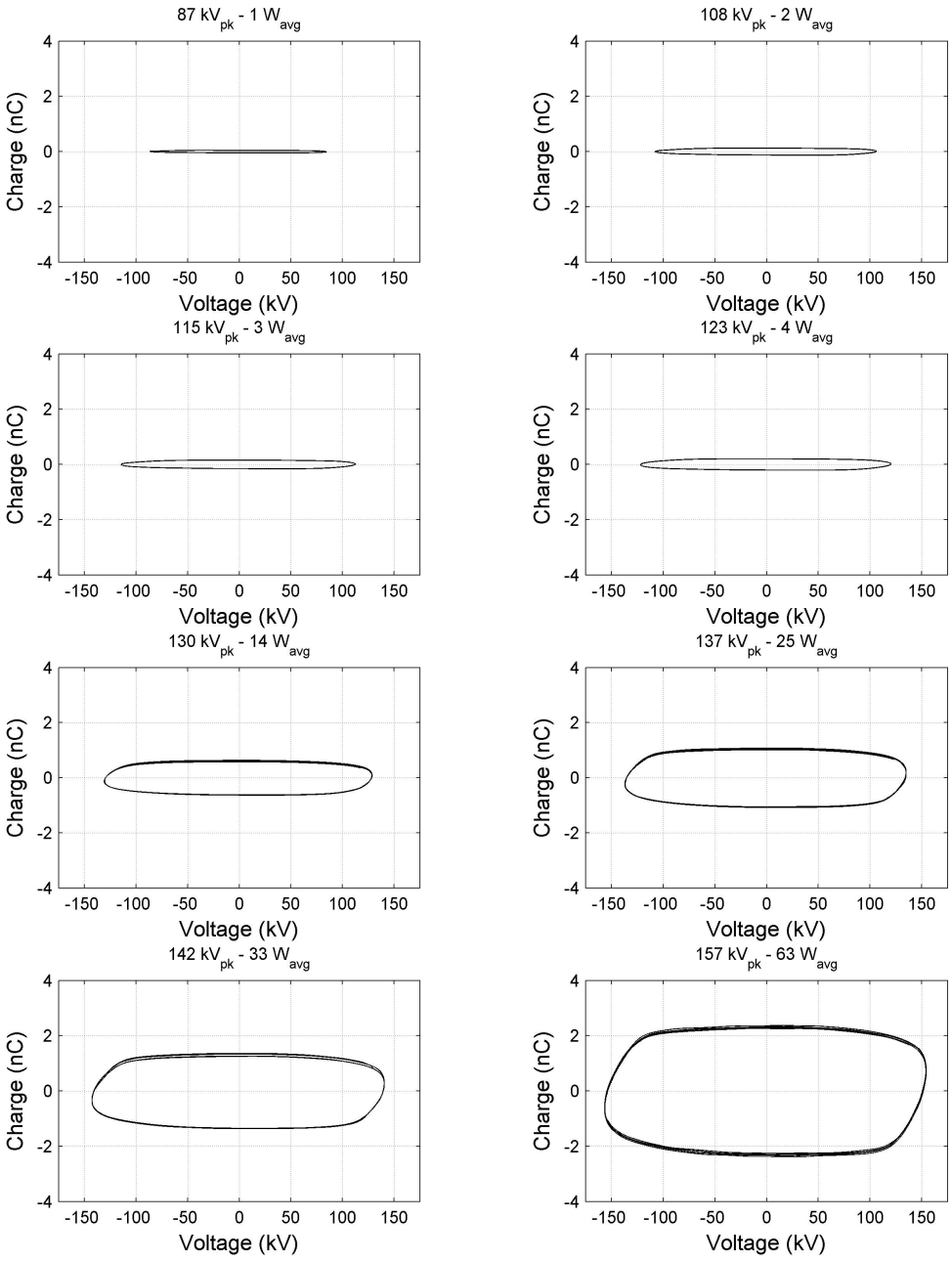

Figure 4.13:
QV-trace development (45 °C)

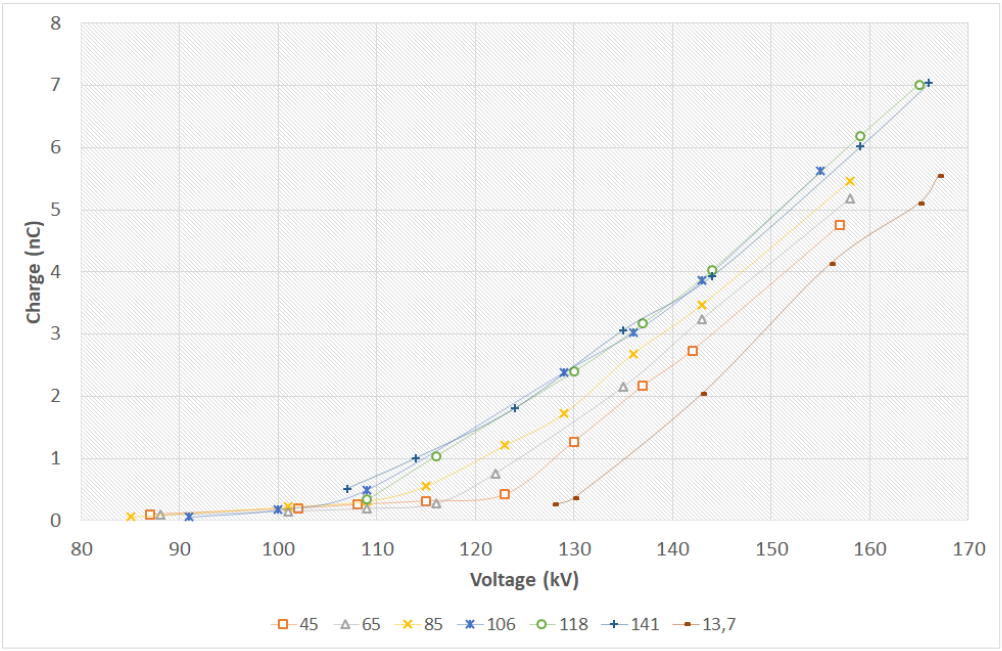

Figure 4.14: Charge vs. Voltage at various tempratures

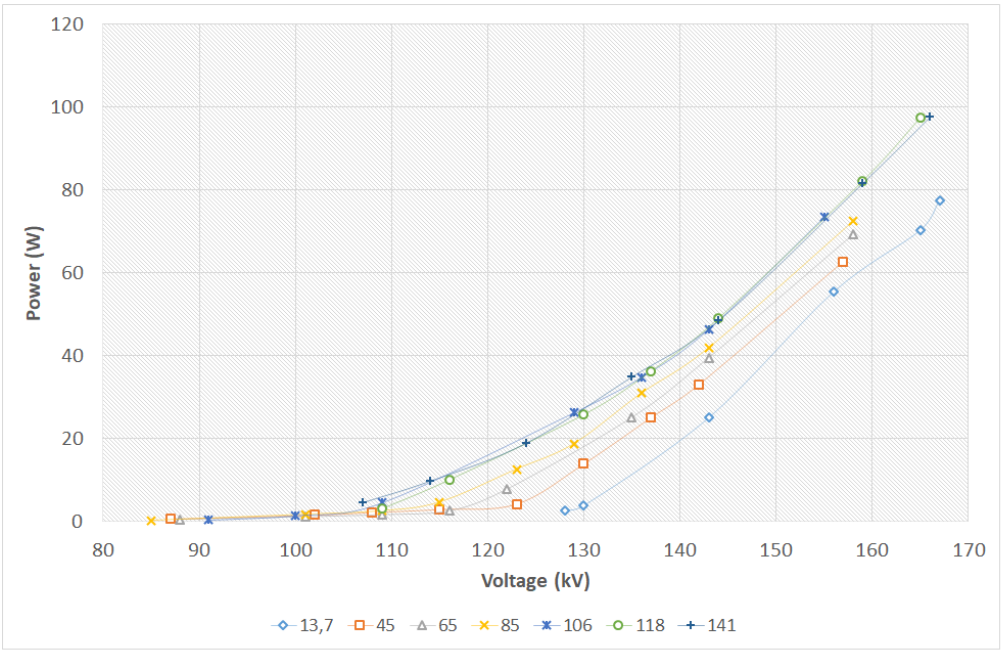

Figure 4.15: Power vs. Voltage at various tempratures

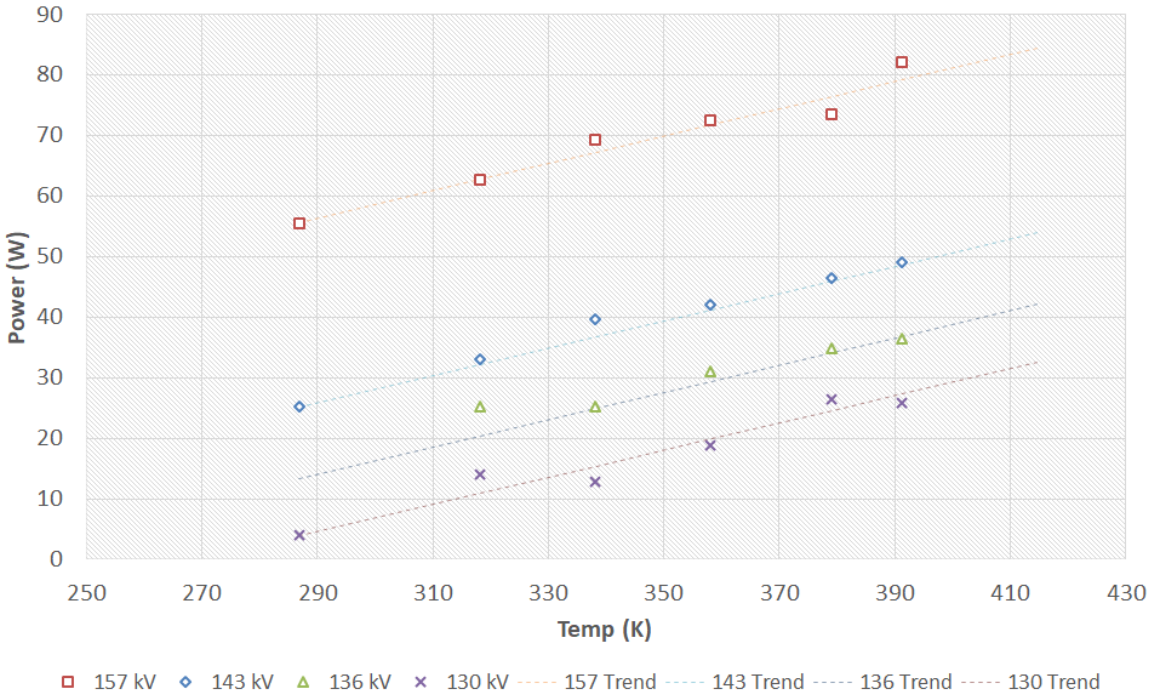

Figure 4.16: Power vs. Temperature at various voltages

5 Discussion

Exploration of results, more detail and meaning, cite relevant sources

5.1 Corona luminous intensity

Recorded images for 140 °C was shown. No analysis was performed, however it was observed that the perceived intensity of the ionisation had increased with the test voltage for all conductor temperatures as expected.

The dominant corona modes were negative (cathodic) trichel discharges and positive (anodic) Hermstein's glow discharges. Even though positive streamers appeared at higher test voltages, they were suppressed by the residual negative ions in the space due to the AC excitation [12]. The residual space charge formed by the strong negative corona, further assisted to enhance the field for anodic discharges, which helped to develop the Hermstein's glow discharges, which appeared in direct proximity to the negative (cathode) discharge spots.

5.2 Observed Corona behavior from measured data and wave shapes

The **voltage waveform** was sinusoidal with low harmonic distortion so that no further analysis was required. The peak voltage was recorded in each case to calculate or display other quantities.

The **charge waveforms** were fairly smooth and a stable display of charge vs. voltage was obtained in the Lissajous figures 4.11, 4.12 and 4.13 which made these figures useful during measurement and post processing analyses. As an example, a clear change could be observed as soon as corona started.

Little to no change occurred at the zero crossings and the highest gradients or charge transfer occurred close to the voltage peaks; see figure 4.5, 4.7 and 4.9. The corona is therefore proportional to the magnitude of the field.

The **current** and consequently the **instantaneous power waveforms** could identify differences between the positive and negative half cycles. Since the measured current consists of electronic as well as ionic components, the measured power does not directly represent the intensity of the anode or cathode coronas respectively (radiation due to ionisation), but rather the power required to displace the charges created by ionisation.

Corona measurements employing oscillographic or partial discharge methods often display a perceived dead zone close to the voltage peaks where it is often assumed that the discharge pulses cease; This behavior may simply be ascribed to local integration or filtering. The power losses during the positive half cycle are generally higher so that the conductor, which is at the opposite polarity, has a net outward flux of negative charges.

Instabilities in the current and power waveforms further aided in identifying if the corona was stable or not as shown in figures 4.6 to 4.10. It can be shown that the power trace is erratic at the start, smoothing out and then again becoming erratic. This is due to the different corona modes ranging from unstable glow, to stable glow and finally streamers.

The appearance of excursions (pulses) at the voltage peaks further aid in discrediting the assumption that corona activity at the peaks are diminishing [12], since the displacement of residual charge only, would not result in spurious currents.

5.3 Effect of test voltage on the charge

The load was predominantly capacitive before corona onset and therefore a line with a constant slope was obtained when comparing the measured charge to the test voltage. The slope of the line represents the load capacitance $C = \frac{dQ}{dV}$, but since this displacement current is tuned out by the bridge circuit, a horizontal line resulted after balance.

After corona inception, the line trace opened and the Lissajous figures again had slanted sides with fairly constant slopes (see figure 4.13). In addition, almost straight lines are obtained when graphing the peak to peak charge against the peak test voltage for different temperatures as in figure 4.14.

These slopes may be interpreted as a non-linear conductance or a capacitance.

Capacitive model: This charge vs. voltage behaviour after inception is similar to that documented for stator bar loss measurements using similar bridge circuits 3.9 and is often interpreted as a change in the capacitance of the circuit, where the slope represents the change in capacitance or ΔC, so that:

$$\frac{dQ}{dV} = \Delta C = C_{new} - C_{old} \tag{24}$$

C_{old} and C_{new} represents the total load capacitance before and after corona inception respectively. In composite insulation systems, consisting of solid materials and gas gaps, it can be assumed that the gas volumes or gaps are shorted out during breakdown so that the ratio of the volumes are proportional to the capacities as deduced by Dakin [38]:

$$\frac{Air \quad volume}{Solid \quad volume} = \frac{\Delta C}{\epsilon C_{old}} \tag{25}$$

When this model for a "shorted out" or conductive zone is adopted for a homogenous insulation, the approximate radius r of the ionised zone can be calculated from the equality (24) and the standard capacitance formula for coaxial conductors with outer radius b, inner conductor radius a and ionised or conductive zone radius r so that:

$$\begin{aligned}\Delta C &= C_{new} - C_{old} \\ &= 2\pi\epsilon(\frac{1}{\ln\frac{b}{r}} - \frac{1}{\ln\frac{b}{a}})\end{aligned} \tag{26}$$

Since the average slope of the lines in figure 4.14 is $0,097 \quad \frac{pC}{V}$, the capacitance $\Delta C = 0,0485 \quad pF$, when considering that the charge relates to the peak to peak value of the voltage and not the peak value as graphed. Solving for r by entering the values $b = 400\,\text{mm}$ and $a = 7\,\text{mm}$ gives a radius $r = 7.1\,\text{mm}$ or an effective ionisation zone of $0.1\,\text{mm}$.

This radius is not useful as it clearly does not represent the discharge zone and therefore, the capacitance value thus obtained should rather be considered as the additional charges bound at the conductor boundary per volt. Stated differently: an increase in the voltage stress would create more corona and hence more free charges close to the conductor. These free charges would bind additional charge at the conductor boundary just as a solid dielectric would and creates a monotonic increase in charge for an increasing voltage.

Conductance model: Since the charge is derived from the current, $Q = \int idt$, the straight line may also represent a non linear leakage conductance G_c which depends on the rise of potential above the corona inception voltage.

J.S. Townsend [14] stated in his paper of 1915 that this rise in potential is directly proportional to the corona current for coaxial conductor arrangements having glow corona. He derived an equation, also referred to as Townsends quadratic formula, with ΔU the rise in potential U above the inception value U_0, corona current i and the coaxial conductor radii a (inner) and b (outer) respectively:

$$\Delta U = U - U_0 = \frac{ib^2 \ln b/a}{2kU_0} \tag{27}$$

Since a,b,k and U_0 are constants, the relationship can be further simplified to:

$$\begin{aligned}\Delta U &= \frac{i}{k_2} \quad if \quad (U > U_0) \\ then \quad i &= k_2 \Delta U\end{aligned} \tag{28}$$

The constant k_2 may be interpreted as a conductance G_c which is dependent on the rise in potential above corona inception as stated.

In figure 4.14 the charge can be represented as a linear function with a slope g_1 for voltages higher than the inception voltage $Q_{p-p} = g_1 \Delta U$ and since the charge is equivalent to the mean current this function is analogous to (28) and the slope g_1 is proportional to the load conductance for values of $U > U_0$.

5.4 Effect of test voltage on the power

If the corona discharges in a system is modeled as a fixed conductance for voltages exceeding the corona inception threshold as in the previous section, then the power can be expected to have a quadratic function:

$$P_{CL} = \Delta U \cdot i \tag{29}$$

Substitution of (28) yields:

$$P_{CL} = k_2 \cdot \Delta U^2 = G_c \cdot \Delta U^2 \tag{30}$$

The measured data of figure 4.15 shows a quadratic relationship for the power at voltages exceeding a certain threshold similar to the findings of [40], [41]and [42] for AC and DC corona cage experiments.

For the measured data, the power increases gradually after corona inception, until a specific threshold is reached. Observations made during the experiment confirmed that this threshold coincides with the rapid development of corona on the conductor and not with the first appearance of corona discharges. In all cases where the corona was well established, anode glow or Hermstein's glow was present.

Inception prediction:

The predictions made by Holtzhausen, Pieterse and Vermeulen in [4] using Peek's formula and the conductor temperature to calculate the local air density, showed a good fit with the measured data, when they defined the occurrence of three or more corona sources or the point of rapid change as the corona inception voltage.

The predicted corona inception field vs. conductor temperature for this model is shown in figure 5.1,"Peek...", along with the measured values using the ICCD camera ,"inception", and the values where the power changes abrubtly ,"Power inception.

A monotonically decreasing "inception" voltage results for an increase in conductor temperature when using the citeria for "full" corona or the threshold voltages where the current and power progresses rapidly. This classification provides a better fit to the Peek model as compared to the data for the first appearance of discharges.

The low inception field values obtained using the ICCD camera, sugests that local disturbances i.e. dust particle play a significant role in the first appearance of corona on he conductor.

Since excitations are less favorable for energetic electrons, the ionisation coefficient α, is lower for higher temperatures which may explain the higher inception voltage for the right side of the data. Toward the left of the curve, the inception voltage also increases. This is probably caused by the lower mean kinetic energy of the electrons which reduces the number

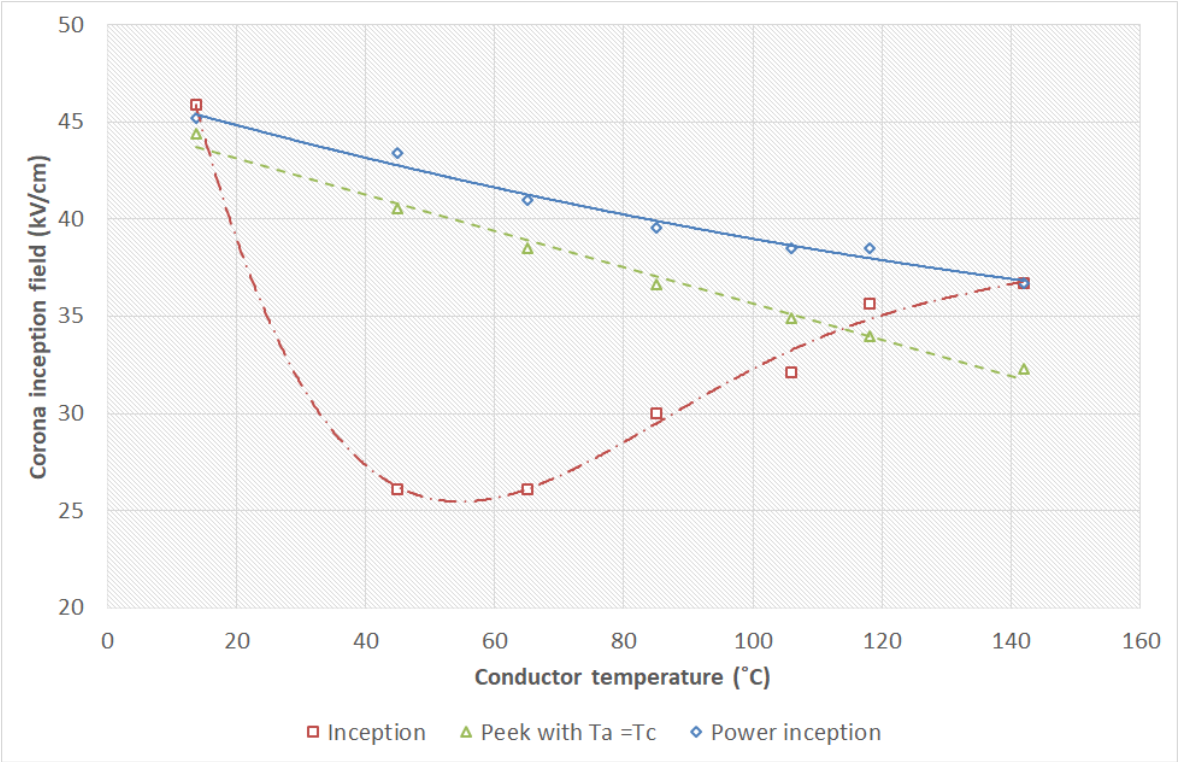

Figure 5.1: Measured corona inception field using ICCD camera and progressive power increase as compared to the predicted Peek values

of electrons released at the cathode and produces lower energy photons during de-excitation or relaxation. As soon as the corona discharges stabilise, a space charge is formed, which disrupts the field creating intense avalanches close to the conductor. Under such conditions it is probable that photo-ionisation and secondary emmissions will increase, so that higher energy electrons or a higher conductor temperature would reduce the inception field strength. It can therefore be deduced that secondary emissions and photo-ionisation are the dominant sustaining mechanisms as soon as corona occurs uniformly on the conductor or a residual space charge is formed.

5.5 Effect of temperature on the power

As shown in figure 4.16 the power losses increase steadily with temperature for fixed voltages and the slope of all the fit lines are close to the same value i.e. 0.225. For the measured temperature range of 14 °C to 140 °C the Power had increased twofold. Figure 5.2 from [1] shows an increase of $5dB\mu V/m$ to $10dB\mu V/m$ in the temperature range, −6 °C to 50 °C which equates to an approximate doubling of the corona intensity ($6dB\mu V$). Furthermore, they have found the Audible noise to increase by almost $10dBA$ which equates to a doubling of the perceived loudness. These results imply that different geometries and test voltage types

present different slopes which requires further study; however the linear behaviour for the two different arrangements implies that a simple model can be developed. A general equation of the form:

$$P_T = P_0 + k(T - T_0) \tag{31}$$

can be sugested where P_T is the Power loss at conductor temperature T, $k = 0.225$ is a proportional constant related to the geometry and P_0 is the power loss at standard temperature T_0. Due to insufficient data, a complete model can not be attained and therefore further work is required.

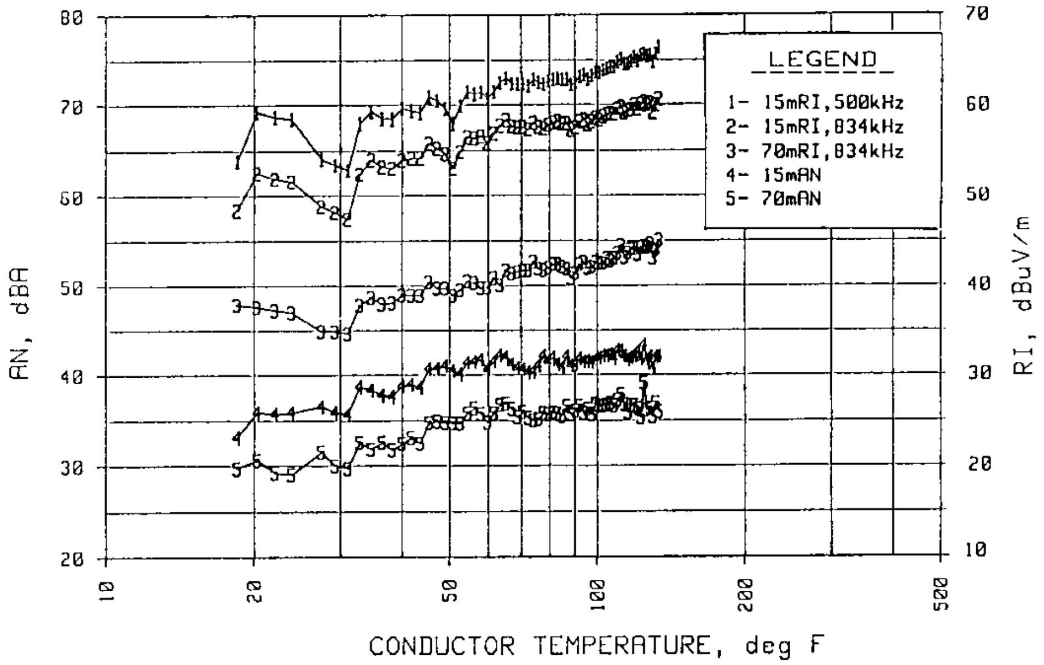

Figure 5.2: RI and AN vs. conductor temperature [1]

6 Conclusion

In conclusion, this dissertation explores power line Corona, shedding light on its complex behavior and various discharge forms. Section 2.4 introduces power line Corona as an electrical discharge occurring under specific gas ionization conditions, manifesting in diverse discharge forms which can be grouped into glow and streamer (brush-like) discharges. The necessary processes in both the gas and at the cathode to establish and sustain ionization have been elucidated.

Importantly, air density emerges as a key influence on gas processes, lowering ionization thresholds. Various processes affecting the secondary feedback mechanism at the cathode have been discussed. While the classical thermionic process was deemed insignificant, the effect of conductor temperature on electron energy probability distribution, especially in reducing the energy required to release electrons from the conductor surface, cannot be ignored. Even though the presence of an aluminum oxide layer was found to increase the photoelectric work function, it could also increase the surface charge, potentially leading to field emissions. These feedback effects, challenging to isolate, often culminate in deriving a single feedback constant λ. Since most of these mechanisms are influenced by the geometrical distribution of gas ions, atoms, photons and metastables, it is likely that a reduced gas density will augment collisions at the cathode, releasing more secondary electrons at the metal surface.

The most significant adverse effects of corona were identified as radio interference, audio noise, and power losses. However, limited investigations have evaluated these nuisances for hot conductors, with a predominant focus on radio and audible noise. Particularly, since these factors have the highest impact on design acceptance for rural areas. Concerning power losses, fair weather corona losses remain considerably lower than foul weather corona losses which may even be reduced by higher conductor temperatures [35], [36] so that the effect of hot conductors on power losses was generally ignored. Despite the renewed interest in the topic, born out of the necessity for compact lines and the utilization of high-temperature low sag conductors, scant published work exists for temperatures surpassing typical maximum operating temperatures of 75 °C.

The first systematic study investigating the effect of conductor temperature on corona inception voltage dates back to 1980 [33]. Subsequent studies in 1990 e.g. [1] delved into the effects of conductor temperature on audible noise and radio interference, primarily focusing on low temperatures ranging from −8 °C to 55 °C. While some initial findings on radio interference and corona current measurement were presented in an EPRI [9] working committee meeting for higher temperatures, they have not been published. Our own research initially concentrated on visual corona inception voltage; however, realizing its inability to quantify severity and considering the influence of temperature on cathode spots' visual appearance, alternative methods were explored to determine corona severity within a small corona cage.

Chapter 3 discussed the limitations of digital sampling methods and Schering bridge methods, particularly in small corona cages. It introduced the charge integration bridge and proposed further circuit adaptations to enhance safety and symmetry in the displayed ellipse. While this bridge doesn't aim for precision, calibration with a charge calibrator demonstrated an impressive accuracy of over 99 %. Consequently, a novel test method was devised using this bridge in a small corona cage setup to study the effects of conductor temperature on corona. This involved employing an inverted test cage geometry with the conductor grounded, allowing simple measurement of voltage and corona current while concurrently heating the conductor with an AC current.

During testing, the voltage and charge integral were displayed on an oscilloscope, providing unambiguous corona inception detection. The bridge could be balanced at low test voltages to display a flattened ellipse that would open with the onset of significant corona currents. Test data was meticulously captured, and post-processing methods were demonstrated to extract the charge integral (average current) and peak power for each half cycle independently, as well as the average power over the sampling interval.

Significantly, the results showcased a nearly linear reduction in inception voltage with an increase in conductor temperature 5.1, likely due to the reduced gas density. Post corona inception, a further increase in test voltage led to a linear charge increase and a quadratic increase in power losses. Additionally, an increase in conductor temperature shifted the x-intercept of the charge vs. voltage function 4.14 and the vertex of the power vs. voltage plot 4.15 to the left, preserving the slope and scale of the charge and power curves, respectively. This fixed slope can be modelled as a fixed conductance, dependent on conductor geometry and properties, as deduced from Townsend's quadratic formula 27. Alternatively, it may be interpreted as a sudden change in capacitance as new charge carriers form in proportion to the voltage exceeding the inception value. The latter provides an unsatisfactory physical model and therefore it may simply be deduced that an increase in the field intensity or the work done (voltage) creates a proportional increase in the charge carriers due to a higher ionisation probability. Regardless of the model assumed, it's evident that the glow regime dominates at higher temperatures, as evidenced by the fixed conductance in glow discharges according to Townsend [14].

Moreover, an increase in conductor temperature yielded a steady increase in corona power loss. The slope of the line remained essentially constant for different test voltages, allowing the derivation of a simple function to predict power losses at higher temperatures. Similar results were found in previous studies [1] for tests at much lower temperatures, suggesting the possibility of extrapolation over a wider temperature range. However, the slope of the line is geometry and material specific, necessitating further research to develop a satisfactory model.

In summary, this research validates the initial hypothesis and highlights the applicability of capacitive bridge methods, offering a simple inception detection method and enabling the display of charge displacement and net charge movement in each half-cycle. These methods can be easily calibrated with state-of-the-art pulse calibrators and provide a straightforward measurement of current and power using post-processing techniques. Importantly, an increase in conductor temperature was observed to reduce the inception voltage while amplifying the dominance of the glow mode at higher temperatures. The conductance of the discharge remains constant and unaffected by temperature, while corona loss exponentially increases (quadratic) with voltage. Moreover, the power curve shifts to the left for higher temperatures, causing a higher loss at a specific voltage. The corona loss will increase linearly at a constant slope for higher temperatures, and a simple function can be derived to predict this behavior. These comprehensive insights contribute significantly to the understanding of power line Corona and its implications on electrical systems, paving the way for further research and optimized power transmission systems.

7 References

[1] V. Chartier and R. Stearns, "Examination of grizzly mountain data base to determine effects of relative air density and conductor temperature on hvdc corona phenomena," *IEEE Transactions on Power Delivery*, vol. 5, pp. 1575–1582, 1990.

[2] F. W. Peek, *Dielectric phenomena in High Voltage Engineering.* McGraw Hill, 1929.

[3] J. Cobine, *Gaseous Conductors: Theory and Engineering Applications.* McGraw-Hill book Company, Incorporated, 1941.

[4] J. P. Holtzhausen, P. J. Pieterse, and H. J. Vermeulen, "Investigation of the effect of conductor temperature on ac power line corona," *2010 International Conference on High Voltage Engineering and Application, ICHVE 2010*, pp. 96–99, 2010.

[5] J. Holtzhausen, P. Buckle, P. Pieterse, and H. Vermeulen, "An experimental investigation into the effect of conductor temperature on ac power line corona," *23rd Southern African Universities Power Engineering Conference*, pp. 300–304, 2010.

[6] P. J. Pieterse, "Corona measurement in an inverted coaxial geometry to evaluate the effect of conductor temperature," *23rd Southern African Universities Power Engineering Conference*, 2014.

[7] G. J. Reid and H. J. Vermeulen, "Effects of conductor temperature on corona inception," *Proceedings of the Universities Power Engineering Conference*, 2014.

[8] P. J. Pieterse and J. M. Strauss, "Corona loss measurement using a capacitance bridge with a zero crossing reset circuit," *25th Southern African Universities Power Engineering Conference*, 2016.

[9] J. Chan, "Corona performance of conductors at high temperatures," *IEEE PES Joint Technical Committee Meeting (Presentation)*, 12 January 2009.

[10] L. Loeb, *Electrical Coronas, Their Basic Physical Mechanisms.* Univ. of California Press, Berkeley, 1965.

[11] E. Nasser, *Fundamentals of gaseous ionization and plasma electronics.* John Wiley and Sons, 1971.

[12] T. N. Giao and J. B. Jordan, "Modes of corona discharges in air," *IEEE Transactions on Power Apparatus and Systems*, vol. PAS-87, 1968.

[13] B. Bleaney and B. Bleaney, *Electricity and Magnetism.* Oxford University Press, 1957.

[14] J. S. Townsend, "Electricity in gases," *Journal of the Röntgen Society*, vol. 11, 1915.

[15] R. J. E. Clausius, "On the mean lengths of paths de- scribed by separate molecules of gaseous bodies," *Annalen der Physik*, vol. 105, p. 239–258, 1858.

[16] J. Thomson, "Xlii. ionization by moving electrified particles," *The London, Edinburgh, and Dublin Philosophical Magazine and Journal of Science*, vol. 23, 1912.

[17] W. Rogowski, "Rückwirkung durch metastabile atome und durchschlagssenkung bei edelgasen," *Zeitschrift für Physik*, vol. 115, pp. 257–295, 5 1940. [Online]. Available: https://link.springer.com/article/10.1007/BF01329821

[18] R. W. Engstrom and W. S. Huxford, "Time-lag analysis of the townsend discharge in argon with activated caesium electrodes," *Physical Review*, vol. 58, p. 67, 7 1940. [Online]. Available: https://journals.aps.org/pr/abstract/10.1103/PhysRev.58.67

[19] L. Malter, "Anomalous secondary electron emission a new phenomenon," *Physical Review*, vol. 49, p. 478, 3 1936. [Online]. Available: https://journals.aps.org/pr/abstract/10.1103/PhysRev.49.478

[20] Wikipedia. Electronic band structure. [Online]. Available: https://en.wikipedia.org/wiki/Electronic_band_structure

[21] A. Einstein, "Über einen die erzeugung und verwandlung des lichtes betreffenden heuristischen gesichtspunkt," *Annalen der Physik*, vol. 322, pp. 132–148, 1 1905. [Online]. Available: https://onlinelibrary.wiley.com/doi/full/10.1002/andp.19053220607

[22] O. Richardson, "The emission of electricity from hot bodies," *Nature 1916 98:2452*, vol. 98, pp. 146–146, 10 1916. [Online]. Available: https://www.nature.com/articles/098146a0

[23] R. H. Fowler and L. Nordheim, "Electron emission in intense electric fields," vol. Vol. 119, no. 781, pp. 173 – 181.

[24] R. H. Good and E. W. Müller, "Field emission," pp. 176–231, 1956. [Online]. Available: https://link.springer.com/chapter/10.1007/978-3-642-45844-6_2

[25] A. V. Kozyrev, V. Y. Kozhevnikov, I. D. Kostyrya, D. V. Rybka, V. F. Tarasenko, and D. V. Schitz, "Radiation from a diffuse corona discharge in atmospheric-pressure air," *Atmospheric and Oceanic Optics*, vol. 25, pp. 176–183, 4 2012. [Online]. Available: https://link.springer.com/article/10.1134/S102485601202008X

[26] R. Vanselow, "Field electron emission from an aluminum oxide covered tungsten (112) plane at temperatures up to 1700°k," *Applied Physics*, vol. 2, pp. 229–235, 11 1973. [Online]. Available: https://link.springer.com/article/10.1007/BF00889504

[27] J. B. Whitehead, "The high voltage corona in air," *Proceedings of the American Philosophical Society*, vol. 59, no. 4, pp. 245–260, 1920. [Online]. Available: http://www.jstor.org/stable/984424

[28] B. Cozzens, "Corona loss measurements for the design of transmission lines to operate at voltages between 220 kv. and 330 kv." *Transactions of the American Institute of Electrical Engineers*, vol. 52, pp. 55–62, 1933.

[29] L. M. Robertson and J. K. Dillard, "Leadville high-altitude extra-high-voltage test project: Part i—report on 4 years of testing," *Transactions of the American Institute of Electrical Engineers. Part III: Power Apparatus and Systems*, vol. 80, pp. 715–723, 1961.

[30] L. B. Loeb, *Basic Processes of Gaseous Electronics*. Univ. of California Press, Berkeley, 1955.

[31] G. W. Trichel, "The mechanism of the negative point to plane corona near onset," *Physical Review*, vol. 54, p. 1078, 12 1938. [Online]. Available: https://journals.aps.org/pr/abstract/10.1103/PhysRev.54.1078

[32] P. L. Morton, "Ionization currents in non-uniform electric fields," *Physical Review*, vol. 70, p. 358, 9 1946. [Online]. Available: https://journals.aps.org/pr/abstract/10.1103/PhysRev.70.358

[33] V. T. Morgan and R. Morrow, "Cooling of a heated cylinder in still air by electrical corona," *Inst. Eng. Aust. Electr. Eng. Trans*, vol. EE16, p. 15, 1980. [Online]. Available: http://hdl.handle.net/102.100.100/294294?index=1

[34] L. B. Loeb, A. F. Kip, G. G. Hudson, and W. H. Bennett, "Pulses in negative point-to-plane corona," *Physical Review*, vol. 60, pp. 714–722, 1941.

[35] P. S. Maruvada, *Corona Performance of High-Voltage Transmission Lines*. Research Studies Press Ltd., 2000.

[36] V. Chartier, "Effect of load current on conductor corona," *Cigre Study comitee 36*, 1993.

[37] "Survey on the use of compact overhead lines: Results and analysis." [Online]. Available: https://www.epri.com/research/products/3002003633

[38] T. W. Dakin and P. J. Malinaric, "A capacitance bridge method for measuring integrated corona-charge transfer and power loss per cycle," *Transactions of the American Institute of Electrical Engineers. Part III: Power Apparatus and Systems*, vol. 79, pp. 648–652, 1960.

[39] T. C. Manley, "The electric characteristics of the ozonator discharge," *Transactions of The Electrochemical Society*, vol. 84, p. 83, 10 1943. [Online].

Available: https://iopscience.iop.org/article/10.1149/1.3071556https://iopscience.iop.org/article/10.1149/1.3071556/meta

[40] C. Eroncel, S. Ilhan, A. Ozdemir, and A. Kaypmaz, "Corona onset voltage and corona power losses in an indoor corona cage," *14th International Middle East Power System Conference (MEPCON'10)*, pp. 791 – 794, 2010.

[41] E. Bousiou, P. Mikropoulis, and V. Zagkanas, "Experimental investigation of negative dc corona on conductor bundles: A comparison with positive corona," *51st International Universities Power Engineering Conference (UPEC)*, 2016.

[42] F. Yin, M. Farzaneh, and X. Jiang, "A capacitance bridge method for measuring integrated corona-charge transfer and power loss per cycle," *The Institution of Engineering and Technology IET Journals - High Volt.*, vol. 2, pp. 102 – 109, 2016.

APPENDIX - Test circuit details

Figure 7.1 shows the test cage pictorially with diagramatical annotations to show the physical connections corresponding to the circuit diagram of figure 7.2.

The outer conductor or the cage was connected to the high voltage terminal U and the centre conductor was connected to terminal B. This conductor was isolated from ground and passed through a current transformer to induce a heating current in it. A low loss capacitor C_1 was connected between terminals U and A as shown. Terminals A and B was passed to the control room using screened coaxial cables and were connected to bridge components as shown in figure 7.2.

Component values: The series resistor $R_s = 2M\Omega$ and the measuring capacitor $C_m = 60pF$ formed a low pass filter. For a standard capacitance $C_1 = 1nF$ and a cage capacitance of approximately $C_2 = 35pF$, the required bridge component values at balance were: , $C_3 = 2.624\mu F$, which consisted of a fixed $2.2\mu F$ capacitor and an external capacitance decade, Resistance decade $R_3 = 80, 6k\Omega$ and the integration capacitance $C_4 = 100nF$.

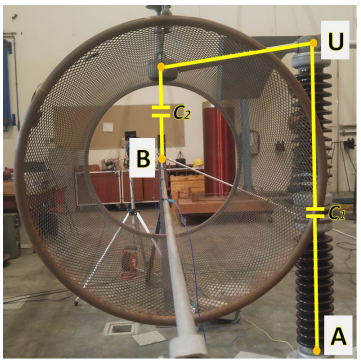

Figure 7.1: Test cage connections

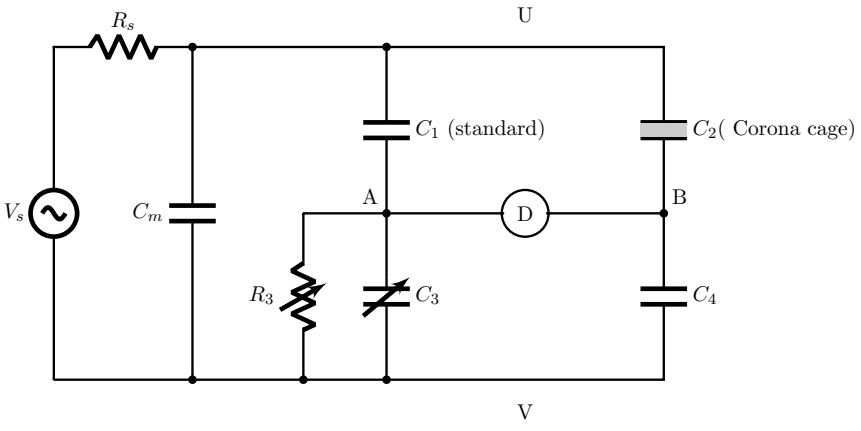

Figure 7.2: Test circuit